JEM Journal of Experimental Medicine

ARTICLE

PDGFA-associated protein 1 protects mature B lymphocytes from stress-induced cell death and promotes antibody gene diversification

Verónica Delgado-Benito[1*], Maria Berruezo-Llacuna[1*], Robert Altwasser[1,2], Wiebke Winkler[3,4], Devakumar Sundaravinayagam[1], Sandhya Balasubramanian[1], Marieta Caganova[3], Robin Graf[3], Ali Rahjouei[1], Marie-Thérèse Henke[5], Madlen Driesner[1], Lisa Keller[1], Alessandro Prigione[5,6], Martin Janz[4], Altuna Akalin[2], and Michela Di Virgilio[1,7]

The establishment of protective humoral immunity is dependent on the ability of mature B cells to undergo antibody gene diversification while adjusting to the physiological stressors induced by activation with the antigen. Mature B cells diversify their antibody genes by class switch recombination (CSR) and somatic hypermutation (SHM), which are both dependent on efficient induction of activation-induced cytidine deaminase (AID). Here, we identified PDGFA-associated protein 1 (Pdap1) as an essential regulator of cellular homeostasis in mature B cells. Pdap1 deficiency leads to sustained expression of the integrated stress response (ISR) effector activating transcription factor 4 (Atf4) and induction of the ISR transcriptional program, increased cell death, and defective AID expression. As a consequence, loss of Pdap1 reduces germinal center B cell formation and impairs CSR and SHM. Thus, Pdap1 protects mature B cells against chronic ISR activation and ensures efficient antibody diversification by promoting their survival and optimal function.

Introduction

The diversity of our Ig gene repertoire is the result of antibody diversification reactions occurring at different stages of B lymphocyte development (Dudley et al., 2005; Methot and Di Noia, 2017). Developing B cells in the bone marrow randomly assemble different gene segments (known as variable, V; diversity, D; and joining, J, genes) at the *Ig* heavy (*Igh*) and light (*Igl*) chain loci via V(D)J recombination (Roth, 2014; Dudley et al., 2005). This process generates unique antibody gene receptors with the potential to collectively recognize a formidable number of antigens. Mature B cells further diversify their *Ig* genes in the periphery via somatic hypermutation (SHM) and class switch recombination (CSR; Pavri and Nussenzweig, 2011; Methot and Di Noia, 2017). SHM introduces point mutations into the variable V(D)J region of the *Ig* genes to generate higher-affinity variants. CSR recombines the *Igh* constant (C) regions to replace the C portion of the IgM heavy chain with one of the alternative isotypes (IgG, IgA, and IgE), thus diversifying the Ig effector function. SHM and CSR are crucial to mount protective humoral responses, as evidenced by primary human immunodeficiency syndromes that are caused by defects in these reactions (Durandy et al., 2013).

SHM and CSR are both dependent on the B cell–specific enzyme activation-induced cytidine deaminase (AID; Revy et al., 2000; Muramatsu et al., 2000). AID deaminates cytosine residues to uracil in single-stranded DNA stretches at the variable regions of both *Igh* and *Igl* loci during SHM, and within special recombining elements (switch [S] regions) of the *Igh* during CSR (Bransteitter et al., 2003; Chaudhuri et al., 2003; Petersen-Mahrt et al., 2002; Pham et al., 2003; Sohail et al., 2003; Ramiro et al., 2003; Dickerson et al., 2003; Matthews et al., 2014; Methot and Di Noia, 2017). The resulting U:G mismatches are differentially processed to generate either mutations in the variable regions or DNA breaks in the S regions (Peled et al., 2008; Methot and Di Noia, 2017; Matthews et al., 2014). AID expression is induced when resting mature (naïve) B cells are activated by the antigen and T cell interactions (Zhou et al.,

[1]Laboratory of Genome Diversification and Integrity, Max Delbrück Center for Molecular Medicine in the Helmholtz Association, Berlin, Germany; [2]Bioinformatics and Omics Data Science Technology Platform, Berlin Institute of Medical Systems Biology, Max Delbrück Center for Molecular Medicine in the Helmholtz Association, Berlin, Germany; [3]Laboratory of Immune Regulation and Cancer, Max Delbrück Center for Molecular Medicine in the Helmholtz Association, Berlin, Germany; [4]Laboratory of Biology of Malignant Lymphomas, Experimental and Clinical Research Center, Max Delbrück Center for Molecular Medicine in the Helmholtz Association and Charité, University Medicine, Berlin, Germany; [5]Laboratory of Mitochondria and Cell Fate Reprogramming, Max Delbrück Center for Molecular Medicine in the Helmholtz Association, Berlin, Germany; [6]Department of General Pediatrics, Neonatology and Pediatric Cardiology, University Children's Hospital, Heinrich Heine University, Düsseldorf, Germany; [7]Charité-Universitätsmedizin Berlin, Berlin, Germany.

*V. Delgado-Benito and M. Berruezo-Llacuna contributed equally to this paper; Correspondence to Michela Di Virgilio: michela.divirgilio@mdc-berlin.de.

2003; Sayegh et al., 2003; Gonda et al., 2003; Cunningham et al., 2004; Dedeoglu et al., 2004; Muramatsu et al., 1999). Antigen stimulation reprograms naïve B cells to exit the quiescent state, expand their cellular biomass, and undergo a proliferative burst within transient and anatomically distinct structures in secondary lymphoid organs called germinal centers (GCs; Cyster and Allen, 2019; Victora and Nussenzweig, 2012). AID expression peaks in GC B cells (Cattoretti et al., 2006; Crouch et al., 2007; Roco et al., 2019). The GC reaction represents the end stage of B cell development, as GC B cells differentiate into memory B cells or long-lived plasma cells that secrete high-affinity antibodies.

The integrated stress response (ISR) is a homeostatic program activated by a variety of physiological and pathological stresses to promote cellular recovery (Ron and Walter, 2007; Pakos-Zebrucka et al., 2016). These stresses include both cell-intrinsic and -extrinsic stimuli, such as ER stress, mitochondrial dysfunction, hypoxia, and amino acid deprivation (Quirós et al., 2017; Harding et al., 1999, 2003; Dever et al., 1992; Rzymski et al., 2010; Ye et al., 2010). All forms of stress converge into the phosphorylation of the α subunit of the eukaryotic translation initiation factor 2 (eIF2α) on serine 51 (Donnelly et al., 2013). This event causes a reduction in global protein synthesis while allowing the preferential translation of few selected genes including the ISR effector activating transcription factor 4 (Atf4; Hinnebusch, 2000; Harding et al., 2000; Scheuner et al., 2001; Lu et al., 2004). Atf4 induces the transcriptional up-regulation of stress-responsive genes and rewires cell metabolism toward the recovery of cellular homeostasis (Harding et al., 2003). The inhibition of general protein translation in the early stage of the ISR is followed by a later phase of translational recovery, which restores protein synthesis once the stress is resolved to support cell survival (Brostrom and Brostrom, 1998; Novoa et al., 2003; Kojima et al., 2003; Marciniak et al., 2004; Brostrom et al., 1989; Ma and Hendershot, 2003).

Although the ISR is an adaptive program meant to restore cellular homeostasis and promote cell survival, under conditions of severe or prolonged stress, it induces cell death by activating proapoptotic pathways (Zou et al., 2008; Puthalakath et al., 2007; Teske et al., 2013; Wang et al., 2009; Ohoka et al., 2005; Gupta et al., 2012; Hiramatsu et al., 2014; Marciniak et al., 2004). Furthermore, the sustained protein synthesis during chronic stress causes proteotoxicity and leads to cell death (Han et al., 2013; Krokowski et al., 2013). Here, we identified Pdap1 as an essential regulator of mature B cell physiology that functions by countering chronic activation of the ISR. Pdap1 ablation in mature B cells causes sustained expression of Atf4, long-term induction of the ISR transcriptional program, and cell death. Furthermore, Pdap1 is essential for efficient induction of AID expression and physiological levels of CSR and SHM.

Results

Pdap1 is required for efficient CSR

To identify novel modulators of mature B cell physiology, we performed loss-of-CSR screens via somatic gene targeting by CRISPR-Cas9 in the B cell lymphoma line CH12. CH12 cells share several properties of resting B cells and have been used to study key aspects of late B cell differentiation, including B cell activation, antibody diversification by CSR, and immunoglobulin secretion (Arnold et al., 1983; Stockdale et al., 1987; Wiest et al., 1990; Corley et al., 1985; Bishop and Haughton, 1986; Nakamura et al., 1996; Ovnic and Corley, 1987; Fagone et al., 2007; Gass et al., 2002; Dufort et al., 2014; LoCascio et al., 1984a, 1984b). Upon cytokine stimulation, CH12 cells express AID and undergo CSR to IgA with high efficiency (Nakamura et al., 1996). CRISPR-Cas9–mediated deletion of factors required for CSR reduces the efficiency of isotype switching in this cell line (Delgado-Benito et al., 2018). Among all tested candidates, targeting of Pdap1 resulted in a considerable reduction of CSR (Fig. 1, A and B). To confirm the results of the loss-of-CSR screen, we generated Pdap1-deficient CH12 clonal derivative cell lines, which included both indel knockout ($Pdap1^{-/-}$) and in-frame deletion mutant ($Pdap1^{mut}$) clones (Fig. 1, C and D). In agreement with the CSR defect observed in bulk CH12 cultures, CSR was impaired in Pdap1-deficient clonal derivatives (Fig. 1 E). We concluded that Pdap1 supports efficient CSR in CH12 cells.

Pdap1 is a 28-kD phosphoprotein highly conserved in vertebrates. It was originally identified as a casein kinase II substrate and a weak interactor of platelet-derived growth factor A (PDGF-A; Shen et al., 1996; Fischer and Schubert, 1996). More recently, Pdap1 was described as an RNA-binding protein in several RNA–protein interactome studies (Castello et al., 2012, 2016; Trendel et al., 2019; Baltz et al., 2012; Iadevaia et al., 2020). However, the precise cellular functions of Pdap1 and its involvement in adaptive immunity are unknown.

To verify Pdap1 involvement in CSR in vivo and elucidate the underlying mechanism, we generated a mouse model bearing a conditional $Pdap1^{F}$ allele and bred it to $Cd19^{Cre/+}$ mice to specifically ablate Pdap1 expression at the early stages of B cell differentiation (Rickert et al., 1997; Fig. S1, A and B). B cell development was largely unaffected in $Pdap1^{F/F}Cd19^{Cre/+}$ mice (Fig. S1, C and D). Although incomplete $Cd19^{Cre}$-mediated recombination of $Pdap1^{F}$ in B cell progenitors could still mask a potential phenotype, these results suggest that Pdap1 is dispensable for V(D)J recombination and early B cell differentiation. However, we observed a pronounced reduction in the number of splenic resting mature B cells (Fig. S1 E). To confirm the intrinsic CSR defect caused by Pdap1 deficiency, we isolated resting splenocytes from $Pdap1^{F/F}Cd19^{Cre/+}$ mice and monitored their capability to undergo CSR upon in vitro stimulation. We assessed CSR under conditions that induce switching to IgG1, IgG3, IgG2b, and IgA and found that Pdap1-deficient B cells displayed reduced levels of CSR for all tested isotypes (Fig. 2, A–D). Western blot (WB) analysis confirmed the near-complete abrogation of Pdap1 expression in these cells (Fig. 2 E). Altogether, these data indicate that Pdap1 is required for efficient CSR in primary B cells irrespective of the stimulation condition.

Pdap1 supports physiological levels of AID expression

CSR is dependent on cell proliferation (Hasbold et al., 1998, 1999; Hodgkin et al., 1996; Deenick et al., 1999). To determine if the reduced CSR efficiency of Pdap1-deficient B cells is caused by an underlying defect in cell proliferation, we monitored the

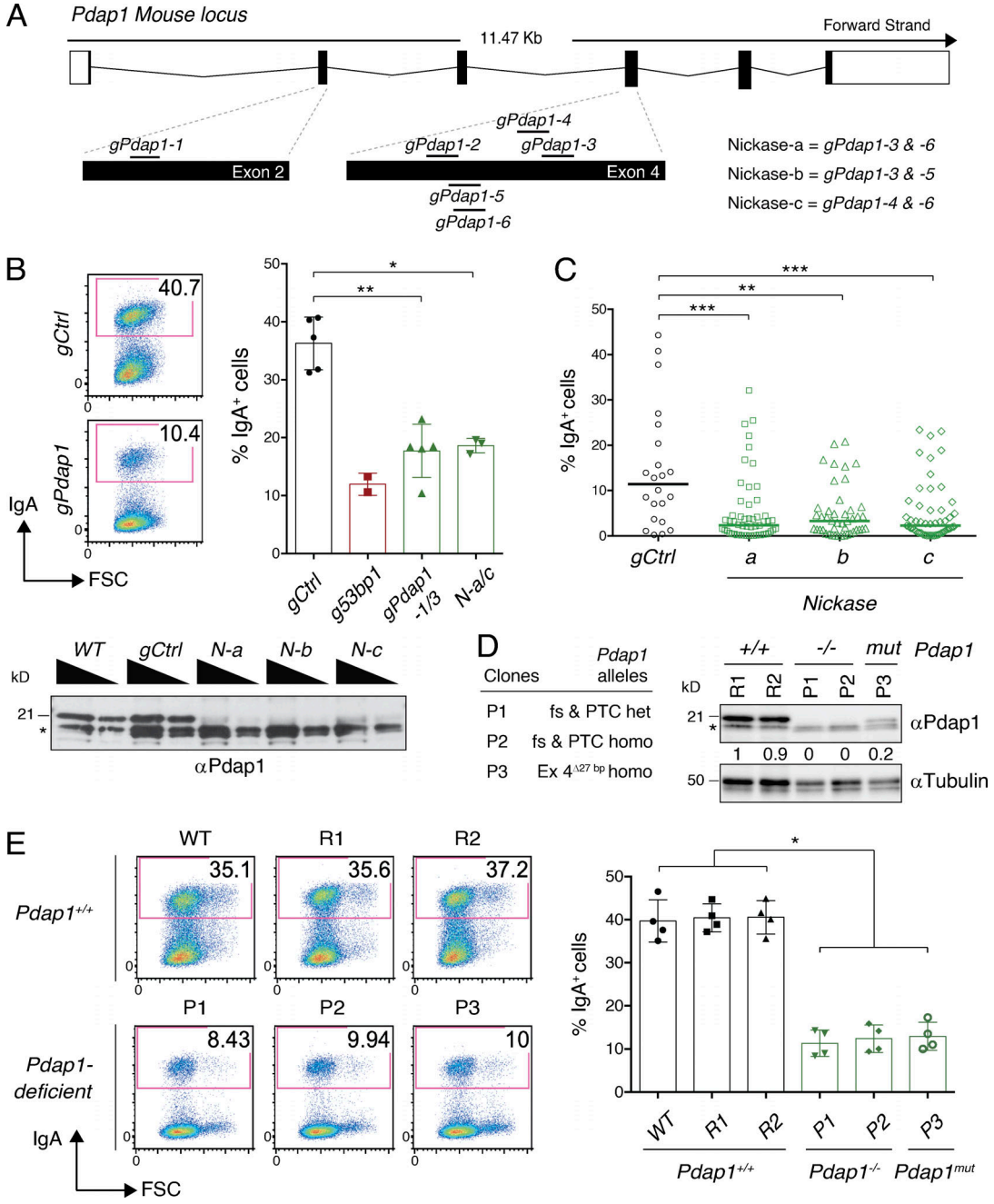

Figure 1. **Loss of Pdap1 in CH12 cells impairs CSR. (A)** Scheme of murine *Pdap1* genomic locus and location of gRNAs used for gene targeting (scheme adapted from Ensembl Pdap1-201 ENSMUST00000031627.8). **(B)** Top left: Representative flow cytometry plots measuring CSR to IgA in activated Cas9/*gPdap1*-nucleofected CH12 cells. Numbers in the plots refer to the percentage of switched cells (= IgA^+ cells). Top right: Summary graph for three independent experiments using *gPdap1-1/3* (individually or in pooled format) or *Nickases-a/c* (individually). Controls for gRNA-nucleofected CH12 were cells electroporated with either empty vector or gRNAs against random sequences not present in the mouse genome (*gCtrl*). A previously described gRNA against the CSR factor 53BP1 (Delgado-Benito et al., 2018) was used as a positive control for loss-of-CSR function. Bottom: WB analysis of whole-cell extracts from CH12 cultures nucleofected with *Nickase-a* to *-c*. Triangles indicate twofold dilution. Asterisk denotes aspecific bands used for internal normalization of protein levels. *N*, *Nickase*. **(C)** Graph summarizing CSR efficiency of activated CH12 clonal cell lines derived by nucleofection of CH12 cultures with *Nickase-a/c* and single-cell sorting. Each symbol in the graphs indicates a single-cell clonal derivative. **(D)** Left: Genomic scars of the targeted alleles in the selected Pdap1-deficient CH12 clonal derivatives. fs, frameshift; PTC, premature termination codon; Δ, bp deletion; het, heterozygous configuration (different indels causing fs and PTC at the two *Pdap1* alleles); homo, homozygous configuration. Right: Representative WB analysis of WT and Pdap1-deficient CH12 cell lines. R1 and R2 are WT clonal derivatives generated by targeting CH12 with random sequences not present in the mouse genome. *mut*, mutated. Asterisk denotes aspecific bands. Numbers underneath the blot indicate relative quantification of Pdap1 signal. **(E)** Left: Representative flow cytometry plots measuring CSR to IgA in activated CH12 cell lines of the indicated genotypes. WT controls included both the parental CH12 cell line (WT) and the random clonal derivatives R1 and R2. Right: Summary graph for four independent experiments. Significance in B, C, and E was calculated with the Mann–Whitney *U* test, and error bars represent SD. *, $P \le 0.05$; **, $P \le 0.01$; ***, $P \le 0.001$.

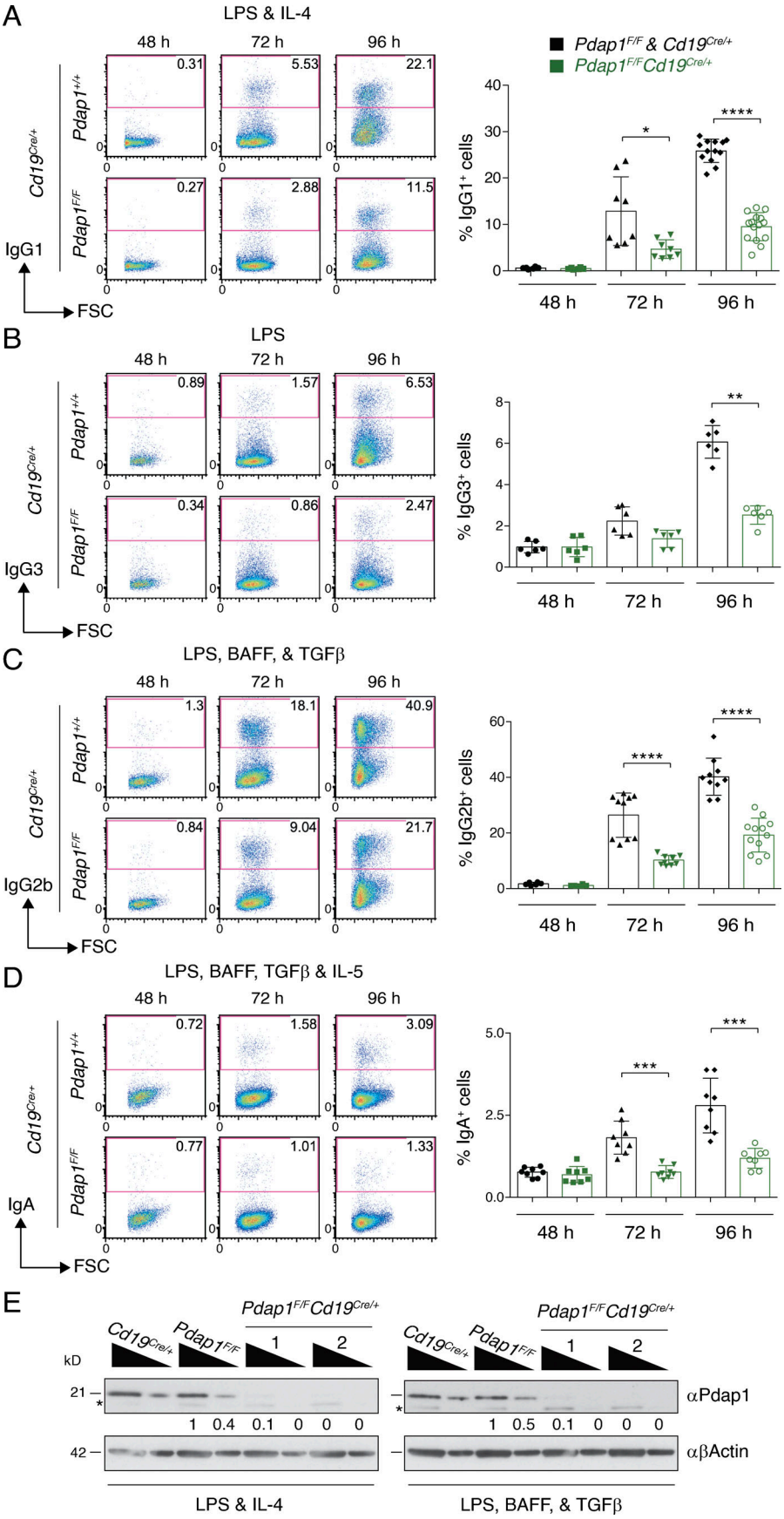

Figure 2. **Pdap1 promotes CSR in primary B cells. (A–D)** Left: Representative flow cytometry plots measuring CSR to IgG1 (A), IgG3 (B), IgG2b (C), and IgA (D) in splenocytes activated with LPS and IL-4 (A), LPS (B), LPS, BAFF, and TGFβ (C), or LPS, BAFF, TGFβ, and IL-5 (D). Numbers in the plots refer to the percentage of switched cells (= IgG1+/IgG3+/IgG2b+/IgGA+ cells). Right: Summary graph for at least six mice per time point per genotype. **(E)** WB analysis of whole-cell extracts from B cells of the indicated genotypes 96 h after stimulation with LPS and IL-4 (left) or LPS, BAFF, and TGFβ (right). 1 and 2 indicate two different *Pdap1F/FCd19Cre/+* mice. Triangles indicate threefold dilution. Asterisk denotes aspecific bands. Numbers underneath the blots indicate relative quantification of Pdap1 signal. Significance in A–D was calculated with the Mann–Whitney *U* test, and error bars represent SD. *, P ≤ 0.05; **, P ≤ 0.01; ***, P ≤ 0.001; ****, P ≤ 0.0001. See also Figs. S1 and S2.

proliferation capabilities of splenocyte cultures by cell tracking dye dilution. The CellTrace Violet dilution profiles of *Pdap1*$^{F/F}$*Cd19*$^{Cre/+}$ B cells were indistinguishable from the control counterparts under all stimulation conditions (Fig. S2, A–D). Furthermore, class switching was reduced in Pdap1-deficient B cells independently of the number of cell divisions (Fig. S2 E). We concluded that Pdap1 is dispensable for B cell proliferation, and that the CSR defect of *Pdap1*$^{F/F}$*Cd19*$^{Cre/+}$ B cells is not due to reduced proliferation capabilities.

The efficiency of CSR is directly linked to the levels of AID expression (Dorsett et al., 2008; Takizawa et al., 2008; Teng et al., 2008). Furthermore, AID targeting is dependent on noncoding transcription across the S regions (germline transcription; GLT), which exposes single-stranded DNA stretches that are the substrate of AID-mediated deamination (Chaudhuri et al., 2003; Dickerson et al., 2003; Ramiro et al., 2003). Therefore, we monitored *Aicda* mRNA and GLT levels in activated B cells by quantitative RT-PCR (qPCR) analysis. We found that *Aicda* transcript levels were consistently reduced in *Pdap1*$^{F/F}$*Cd19*$^{Cre/+}$ B cells compared with controls across all stimulation conditions (Fig. 3 A). Transcription of donor Sμ region was not affected by Pdap1 deletion (Fig. 3 B), whereas acceptor S region transcription exhibited a varied phenotype, with reduced levels of GLTγ1 and GLTα, and minimally affected or unaltered expression for GLTγ3 and GLTγ2b, respectively (Fig. 3 C). Analogously, analysis of *Aicda* and germline transcripts in Pdap1-deficient CH12 cell lines showed reduced *Aicda* mRNA levels but unaffected Sμ and Sα region transcription (Fig. S3, A–C). In agreement with the reduction of *Aicda* mRNA, Pdap1-deficient B cells expressed lower levels of AID protein upon activation compared with control cells (Fig. 3 D).

AID-mediated deamination in the donor Sμ and recombining acceptor S region leads to the formation of DNA double-strand breaks (DSBs), which are ultimately repaired by end joining to ensure productive CSR events (Matthews et al., 2014; Boboila et al., 2012). The reduced AID expression and isotype-specific GLT phenotypes of Pdap1-deficient B cells converge into a pre-DSB defect, since DSB formation at S regions relies on both AID levels and efficient targeting. These results, however, did not exclude the possibility that Pdap1 might play an additional role during CSR downstream break formation, for example in repair of S region DSBs. To test this possibility, we overexpressed AID in Pdap1-deficient B cells and monitored the levels of CSR (Fig. 3 E). To this end, we transduced control and *Pdap1*$^{F/F}$*Cd19*$^{Cre/+}$ splenocytes with a construct expressing AID fused to the hormone-binding domain of the modified estrogen receptor (AID-ER). Provision of 4-hydroxytamoxifen (4-HT) induces the translocation of the cytoplasm-accumulated AID-ER fusion protein into the nucleus and initiates CSR. We found that 4-HT addition rescued the CSR defect of *Pdap1*$^{F/F}$*Cd19*$^{Cre/+}$ cells to levels equivalent to AID-ER–reconstituted *Aicda*$^{-/-}$ splenocytes in cultures stimulated to undergo class switching to IgG2b (Fig. 3 E), which exhibited unaffected GLTγ2b (Fig. 3 C). In contrast, the rescue of CSR was not significant in cells activated to switch to IgG1, with severely reduced GLTγ1 in the absence of Pdap1 (Fig. 3, C and E), and therefore impaired in AID targeting even under conditions of increased AID levels. Altogether, these data indicate that the CSR defect of Pdap1-deficient B cells is caused by impaired formation of AID-induced DSBs, which is caused primarily by reduced AID expression, with the additional contribution of impaired GLT in an isotype-specific manner.

Pdap1 has been recently identified in RNA-protein capture experiments as an RNA binding protein (Castello et al., 2012, 2016; Trendel et al., 2019; Baltz et al., 2012; Iadevaia et al., 2020). Therefore, we considered the possibility that Pdap1 might contribute to the posttranscriptional regulation of AID expression. Because Pdap1 is localized primarily in the cytoplasm (Fig. S4), we first tested whether Pdap1 controls the degradation of *Aicda* mRNA. To do so, we treated *Cd19*$^{Cre/+}$ and *Pdap1*$^{F/F}$*Cd19*$^{Cre/+}$ splenocyte cultures with Actinomycin D to inhibit the de novo transcription of AID and measured *Aicda* mRNA decay by qPCR. We found that depletion of Pdap1 did not affect the kinetics of *Aicda* mRNA degradation (Fig. 4, A and B). This result also indirectly shows that Pdap1 deficiency does not alter decapping or deadenylation of *Aicda* transcripts since a defect in any of these processes would result in accelerated decay. We concluded that Pdap1 is dispensable for *Aicda* transcript stability. Next, we monitored *Aicda* transcript splicing. Several splice variants for AID have been identified, with the full-length transcript being the only splice isoform encoding a functional AID protein (van Maldegem et al., 2009, 2010; Sala et al., 2015). To assess whether Pdap1 modulates *Aicda* splicing, we performed RNA next-generation sequencing (RNA-seq) of activated B cells induced to undergo CSR to either IgG1 or IgG2b and analyzed the pattern of *Aicda* exon usage. We found no difference in the profile of *Aicda* exon usage between *Cd19*$^{Cre/+}$ and *Pdap1*$^{F/F}$*Cd19*$^{Cre/+}$ B cells (Fig. 4 C). Furthermore, primary *Aicda* transcript levels in *Pdap1*$^{F/F}$*Cd19*$^{Cre/+}$ splenocytes were reduced compared with *Cd19*$^{Cre/+}$ cells to an extent similar to that observed for the full-length spliced product (Figs. 4 D and 3 A). We concluded that ablation of Pdap1 does not affect *Aicda* mRNA splicing. Altogether, these findings indicate that Pdap1 supports physiological levels of AID expression, and that the CSR defect of Pdap1-deficient B cells is caused, at least in part, by impaired induction of AID expression following activation rather than a defect in *Aicda* posttranscriptional regulation.

Pdap1 deficiency in B cells induces the Atf4 stress response transcriptional program

To define the mechanism responsible for the defective induction of AID expression in Pdap1-deficient cells, we compared the transcriptome profiles of *Cd19*$^{Cre/+}$ and *Pdap1*$^{F/F}$*Cd19*$^{Cre/+}$ splenocytes stimulated with either LPS and IL-4 or LPS, B cell–activating factor (BAFF), and TGFβ (Table S1). The use of two stimulation conditions allowed us to zoom in common differentially regulated pathways and added a temporal dimension to the experiment, since LPS-BAFF-TGFβ–stimulated splenocytes proliferate faster than LPS-IL-4–activated ones (Fig. S2 F). To identify differentially expressed genes, we set the significance level of false discovery rate (FDR) to <0.05 (Fig. 5 A). The number of differentially regulated genes was higher in LPS-IL-4–stimulated cultures than in LPS-BAFF-TGFβ–activated cells (1,227 versus 173). Furthermore, the number of genes upregulated in *Pdap1*$^{F/F}$*Cd19*$^{Cre/+}$ was considerably higher than the

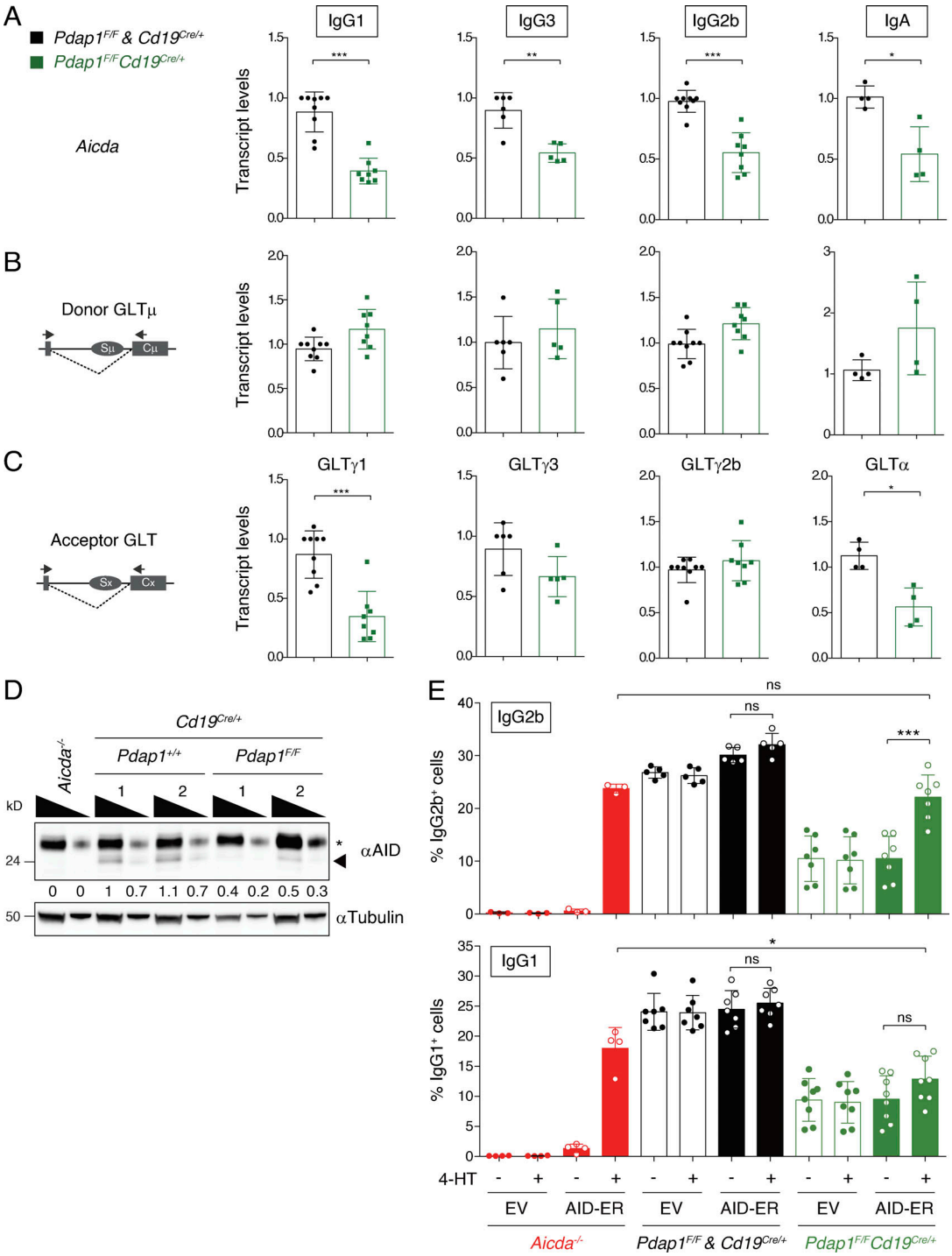

Figure 3. **Pdap1 supports physiological levels of AID expression. (A–C)** qPCR analysis for *Aicda* mRNA (A), Igμ (B), and Igγ1/Igγ3/Igγ2b/Igα (C) GLT levels in B cells activated to undergo CSR to the corresponding isotypes. The schematic representations on the left in B and C indicate the location of primers used to analyze the germline transcripts. Graphs summarize four to eight mice per genotype per stimulation condition. One control mouse (*Cd19*$^{Cre/+}$ or *Pdap1*$^{F/F}$) within each experiment was assigned an arbitrary value of 1. **(D)** Representative WB analysis of splenocytes of the indicated genotypes 48 h after stimulation with LPS and IL-4. 1 and 2 indicate two different mice per genotype. Triangles indicate threefold dilution. Arrowhead and asterisk denote AID and aspecific band, respectively. Numbers underneath the blot indicate relative quantification of AID signal. **(E)** Summary graphs showing CSR to IgG2b (top) and IgG1 (bottom) following transduction of splenocytes of the indicated genotypes with either empty vector (EV) or an AID-ER–expressing retroviral construct. Graphs summarize three to eight mice per genotype analyzed in three (IgG2b) or four (IgG1) independent experiments. Different colors are used to group samples based on genotype (red for *Aicda*$^{-/-}$, black for controls, and green for *Pdap1*$^{F/F}$*Cd19*$^{Cre/+}$). Empty and filled column bars indicate samples infected with EV and AID-ER constructs, respectively. Significance in A, C, and E was calculated with the Mann–Whitney *U* test. Error bars represent SD. ns, not significant; *, P ≤ 0.05; **, P ≤ 0.01; ***, P ≤ 0.001. See also Fig. S3.

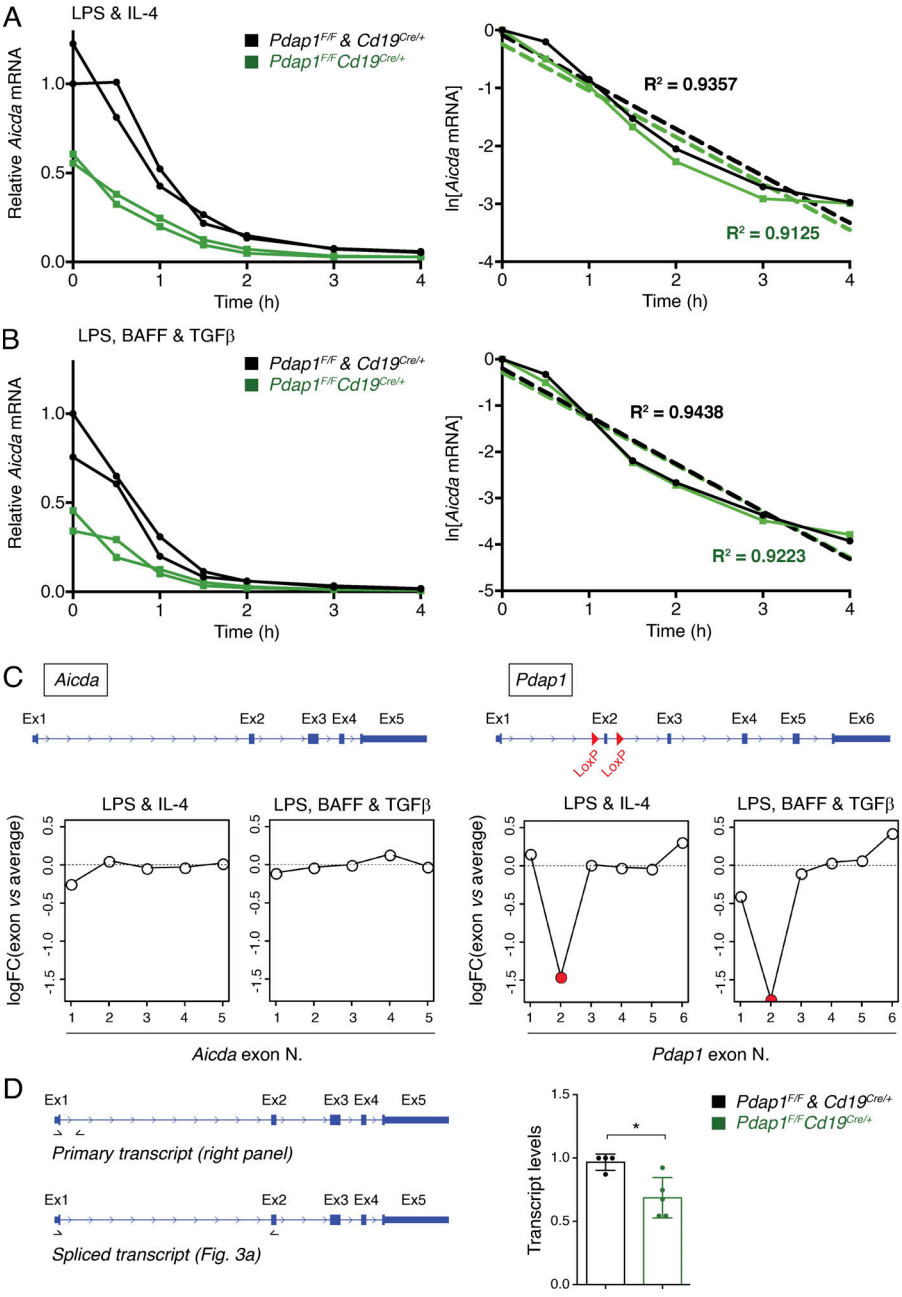

Figure 4. **Pdap1 is dispensable for *Aicda* mRNA stability and splicing. (A and B)** Left: qPCR analysis for *Aicda* mRNA from B cells of the indicated genotypes stimulated with LPS and IL-4 (A) or LPS, BAFF, and TGFβ (B) for 48 h to induce CSR to IgG1 or IgG2b, respectively, and treated with Actinomycin D for the indicated time. Graph summarizes the mean of two independent qPCR measurements per mouse for two mice per genotype. Right: Linear regression analysis of the same data, shown as ln[RNA] versus time of Actinomycin D treatment. **(C)** Analysis of exon usage for *Aicda* (left) and *Pdap1* (right) genes. *Pdap1* splicing data are provided as a positive control for the spicing analysis. A schematic representation of each gene is provided above. **(D)** Left: Schematic representation of *Aicda* gene with location of primers used to analyze *Aicda* primary and spliced transcripts. Right: qPCR analysis of *Aicda* primary transcripts in B cells 48 h after activation with LPS. Graphs summarize at least four mice per genotype. Results of qPCR analysis of *Aicda* spliced transcripts are shown in Fig. 3 A. One *Cd19*$^{Cre/+}$ mouse within each experiment was assigned an arbitrary value of 1. Significance in D was calculated with the Mann–Whitney *U* test, and error bars represent SD. *, P ≤ 0.05.

down-regulated ones in LPS-BAFF-TGFβ–stimulated cultures (124 up- versus 49 down-regulated) but was evenly distributed between the two categories in the LPS-IL-4 stimulation condition (561 up- versus 666 down-regulated).

Pathway enrichment analysis of the down-regulated genes in *Pdap1*$^{F/F}$*Cd19*$^{Cre/+}$ B cells in the LPS-IL-4 dataset identified the protein translation–related categories "ribosome," "ribosome biogenesis in eukaryotes," and "RNA transport" as the most significant categories (Fig. 5 B). Furthermore, analysis of individual genes showed that the most significantly down-regulated ones under both stimulations were factors essential for CSR and/or genes highly expressed or induced in activated B cells (e.g., *Aicda*, *Batf*, *Ccl22*, *Ighg3*, and *Tmem176b*; Fig. 5 C and Table S1). In contrast, the top up-regulated categories in both datasets were related to metabolic pathways of amino acid and aminoacyl-tRNA biosynthesis (Fig. 5 B). Among the most significantly up-regulated genes, we found key enzymes for the biosynthesis of asparagine (*Asns*), cysteine (*Cth*), and serine (*Psat1*, *Psph*), glutathione metabolism (*Chac1*), amino acid transporters (*Slc1a4*, *Slc6a9*), and several other metabolic and cytoprotective genes (Fig. 5 C, Fig. S5 A, and Table S1).

These data indicate that, in addition to the inhibition of key factors of the CSR program, Pdap1 deficiency in activated B cells is accompanied by transcriptional changes that reflect initial repression of global protein synthesis, up-regulation of cellular stress response genes, and metabolic rewiring to aid translational recovery. These changes represent key aspects of the transcriptional program of the ISR (Ron and Walter, 2007; Pakos-Zebrucka et al., 2016). To confirm the activation of the ISR in Pdap1-deficient B cells, we monitored the kinetics of eIF2α

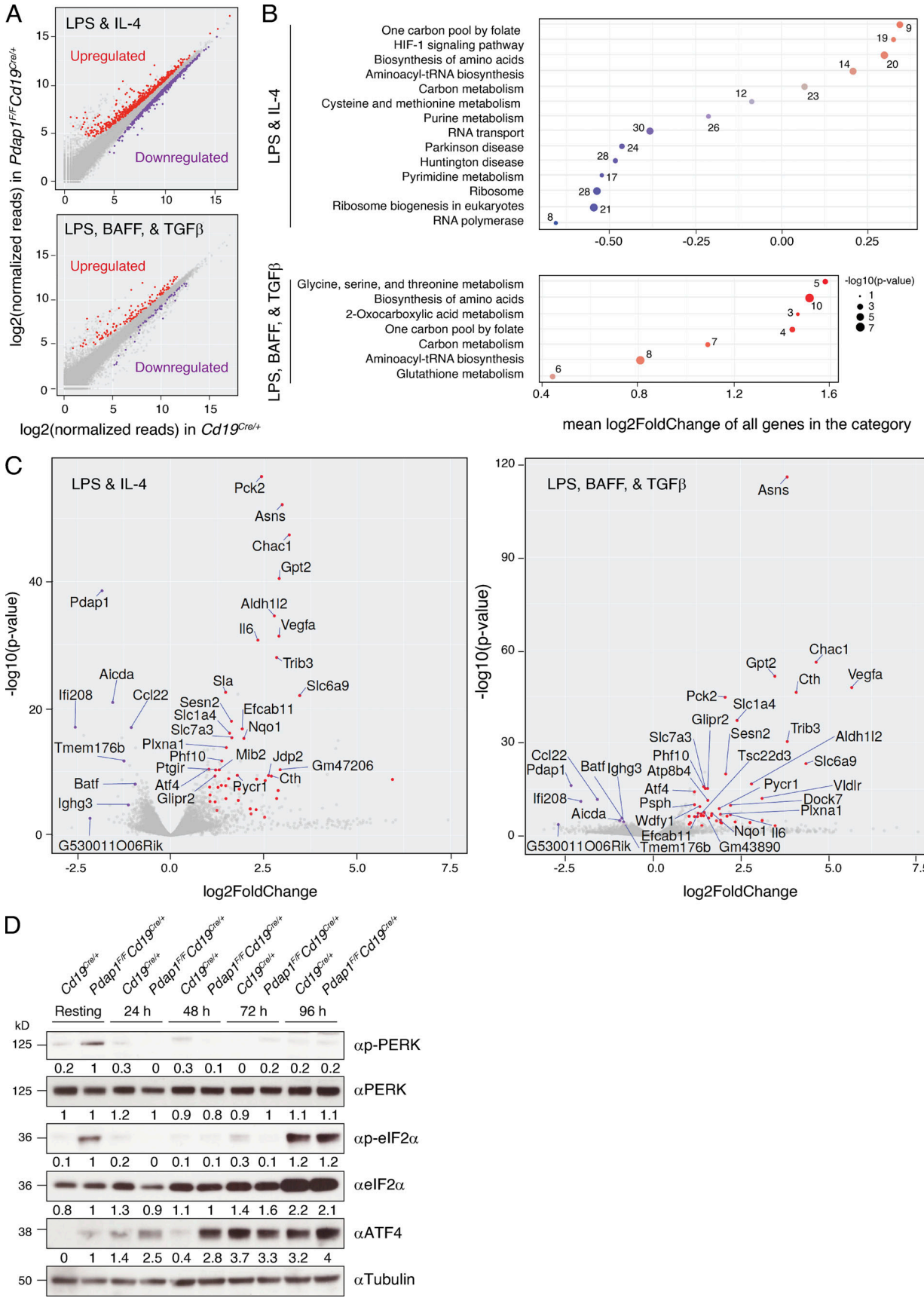

Figure 5. **Pdap1-deficient B cells activate the Atf4 stress response transcriptional program. (A)** Scatterplots of gene expression in *Pdap1*$^{F/F}$*Cd19*$^{Cre/+}$ versus control (*Cd19*$^{Cre/+}$) mature B cells stimulated with LPS and IL-4 (top) or LPS, BAFF, and TGFβ (bottom). Genes with an adjusted P value (FDR) < 0.05 that

are up- or down-regulated in *Pdap1*$^{F/F}$*Cd19*$^{Cre/+}$ cells are highlighted in red or purple, respectively. Data summarizes results from three mice per genotype per stimulation condition and is presented as log2(RPM) (reads per gene per million mapped sequence reads) values. **(B)** Pathway enrichment analysis (KEGG pathways) of the differentially regulated genes (FDR < 0.05) from A. The number of differentially regulated genes in each category is indicated. **(C)** Volcano plots displaying differentially expressed genes between control and Pdap1-deficient splenocytes activated with LPS and IL-4 (right) or LPS, BAFF, and TGFβ (left). The red and purple dots represent transcripts up- and down-regulated in *Pdap1*$^{F/F}$*Cd19*$^{Cre/+}$ cells, respectively, with FDR < 0.05 and expression fold change > 2 (up-regulated) or 1.7 (down-regulated) in both stimulation conditions. The names of the down-regulated and the 30 most significantly up-regulated genes within each stimulation condition are indicated in each graph. The fold change threshold for down-regulated genes was set to 1.7 to include genes yielding a biologically relevant effect even with less pronounced variations in expression levels (e.g., *Aicda*, haploinsufficient gene). **(D)** Representative WB analysis of splenocytes of the indicated genotypes before (resting B cells) and after 24–96-h activation with LPS and IL-4. Data are representative of two mice per genotype, and quantification values of WB signals are indicated underneath the corresponding blots. See also Fig. S5 and Table S1.

phosphorylation and Atf4 expression in resting and in vitro–activated splenocytes. The eIF2α-Atf4 pathway is normally suppressed in splenic B cells and is induced only at later time points after activation, when splenocyte cultures exhibit a general fitness decline (Fig. 5 D and Fig. S5 B, control cells; Zhu et al., 2019). In contrast to control cells, resting B cells from *Pdap1*$^{F/F}$*Cd19*$^{Cre/+}$ spleens displayed a marked phosphorylation of eIF2α and detectable levels of Atf4 protein, thus indicating a baseline activation of the ISR (Fig. 5 D and Fig. S5 B). The ER stress-activated eIF2α kinase PKR-like ER kinase (Perk) also showed autophosphorylation-dependent activation in resting splenocytes (Fig. 5 D and Fig. S5 B). eIF2α phosphorylation was suppressed following activation and was noticeable only in late-stage cultures when eIF2α levels increased considerably in both control and Pdap1-deficient cells (Fig. 5 D and Fig. S5 B). In agreement with a previous report (Zhu et al., 2019), Atf4 was markedly expressed only at late time points after activation in control splenocytes (Fig. 5 D). In contrast, Atf4 protein levels in *Pdap1*$^{F/F}$*Cd19*$^{Cre/+}$ cells increased considerably during the first 24 h after activation from the baseline expression observed in resting B cells (Fig. 5 D). Finally, up-regulation of Atf4 expression in the absence of Pdap1 occurred not only at the translation level but also via transcriptional induction (Fig. 5 C and Fig. S5 A). We concluded that Pdap1 deficiency results in up-regulation of the ISR core component Atf4. Altogether, these data indicate that Pdap1 ablation in mature B cells induces Atf4-dependent expression of stress response genes and down-regulation of the CSR program.

Pdap1 supports survival of mature B cells

The ISR is an adaptive pathway meant to restore cellular homeostasis following cell intrinsic and extrinsic stresses (Harding et al., 1999, 2000, 2003; Brostrom et al., 1996; Dever et al., 1992; Ron and Walter, 2007; Pakos-Zebrucka et al., 2016). However, when the stress is severe in either intensity or duration and overwhelms the response adaptive capacity, the ISR activates the apoptotic cell death program (Pakos-Zebrucka et al., 2016). Furthermore, down-regulation studies have implicated Pdap1 in cell survival and apoptosis resistance of cancer cell lines (Sharma et al., 2016; Weston et al., 2018). Therefore, we tested whether activation of the stress response in the absence of Pdap1 would induce apoptosis in B cells. To do so, we monitored caspase activation in splenocytes by CaspGLOW staining. Caspase activity increased after stimulation and was higher in Pdap1-deficient cells compared with controls at 24 and 48 h after activation (Fig. 6 A). Accordingly, despite the unaffected proliferation capability (Fig. S2), the number of live cells in *Pdap1*$^{F/F}$*Cd19*$^{Cre/+}$ splenocyte cultures was reduced 48 and 72 h after activation (Fig. 6 B). Finally, no differences were detected in mitochondrial mass or respiration capacity compared with controls (Fig. 6 C and Fig. S5 C), thus indicating that activation of the ISR is not caused by mitochondrial disfunction. However, *Pdap1*$^{F/F}$*Cd19*$^{Cre/+}$ cultures displayed an increased proportion of cells with low mitochondrial membrane potential at early time points after activation (24 and 48 h; Fig. 6 D). Hence, a fraction of Pdap1-deficient B cells may undergo mitochondrial depolarization, an event usually associated with apoptosis induction (Gottlieb et al., 2003).

Next, we tested whether Pdap1 deletion would affect the survival of activated B cells in vivo. To this end, we measured the percentage of GC B cells in Peyer's patches of *Cd19*$^{Cre/+}$ and *Pdap1*$^{F/F}$*Cd19*$^{Cre/+}$ mice. Peyer's patches are specialized secondary lymphoid tissues that line the wall of the small intestine. Because of their chronic exposure to an enormous variety of food- and microbiome-derived antigens, Peyer's patches display continual GC activity and are key to the induction of mucosal IgA antibody responses (Reboldi and Cyster, 2016). We found that the percentage of GC B cells was reduced in Peyer's patches of *Pdap1*$^{F/F}$*Cd19*$^{Cre/+}$ mice compared with the control group (Fig. 6 E). In agreement with the CSR defect exhibited by *Pdap1*$^{F/F}$*Cd19*$^{Cre/+}$ splenic B cells following activation in vitro (Fig. 2), the percentage of switched IgA GC B cells was considerably decreased in *Pdap1*$^{F/F}$*Cd19*$^{Cre/+}$ mice (Fig. 6 E). Altogether, these data suggest that Pdap1 is required to support survival of activated B cells.

Pdap1 is dispensable for plasma cell differentiation

Plasma cell differentiation represents the terminal phase of B cell development and is regulated by a transcriptional program that represses B cell identity while promoting the expression of plasma cell signature genes (Nutt et al., 2015; Shi et al., 2015; Minnich et al., 2016). This process is accompanied by massive expansion of the ER and the up-regulation of molecular chaperone and folding enzyme expression. The expansion of the secretory network is essential to accommodate the demands of increased immunoglobulin synthesis and secretion and is dependent on the activation of the unfolded protein response (UPR; Zhang et al., 2005; Gass et al., 2002, 2008; Iwakoshi et al., 2003; van Anken et al., 2003; Shaffer et al., 2004; Taubenheim et al., 2012; Todd et al., 2009). The UPR is a ubiquitous signaling network that senses and responds to the accumulation of misfolded proteins in the ER

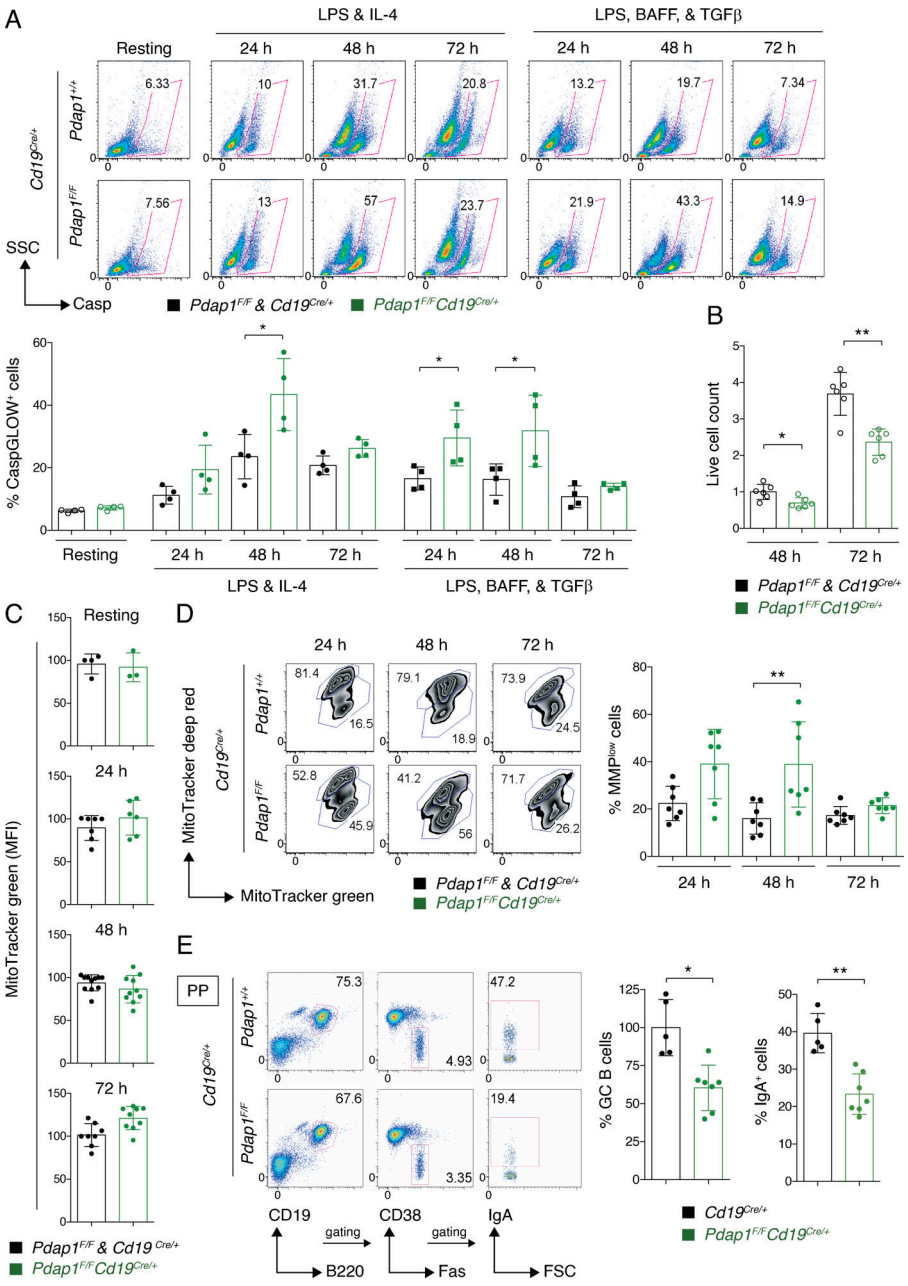

Figure 6. **Pdap1 supports survival of mature B cells. (A)** Top: Representative flow cytometry plots measuring percentage of active caspase$^+$ cells in resting and activated (LPS-IL-4, or LPS-BAFF-TGFβ, 24–72 h) splenocytes of the indicated genotypes. Bottom: Summary graph for four mice per genotype analyzed in two independent experiments. **(B)** Live-cell count of splenocytes of the indicated genotypes activated with LPS and IL-4. Resting B cells were counted and seeded at the same density on day 0. Data summarize three independent experiments for a total of six mice per genotype and are normalized within each experiment to the average of live-cell count for control cultures at 48 h, which was set to 1. **(C)** Mitochondrial mass of resting and LPS + IL-4–activated splenocytes (24–72 h) as determined by MitoTracker green staining and expressed as mean fluorescence intensity (MFI) values. Graphs summarize results from a total of 3–11 mice per genotype analyzed in four independent experiments. **(D)** Left: Representative flow cytometry plots measuring mitochondrial membrane potential (MMP) and mass by MitoTracker deep red and green staining, respectively, in splenocyte cultures of the indicated genotype 24, 48, and 72 h after activation with LPS and IL-4. Right: Summary graph for seven mice per genotype. **(E)** Left: Representative flow cytometry plots measuring percentage of GC B cells and IgA$^+$ GC cells in Peyer's patches (PP) of unimmunized mice. Right: Summary graphs for at least five mice per genotype. Significance in A–E was calculated with the Mann–Whitney *U* test, and error bars represent SD. *, P ≤ 0.05; **, P ≤ 0.01.

(Ron and Walter, 2007; Walter and Ron, 2011; Schröder and Kaufman, 2005). This response is mediated by three ER-resident proteins which, in addition to Perk, comprise the inositol-requiring protein kinase/endoribonuclease-1 (Ire1) and Atf6 (Tirasophon et al., 1998; Wang et al., 1998; Haze et al., 1999, 2001). The UPR ultimately reestablishes protein homeostasis by integrating Perk-eIF2α–dependent attenuation of global protein synthesis with Ire1- and Atf6-mediated transcription of factors and enzymes that increase the protein folding and degradation capabilities of the ER.

The Ire1 and Atf6 branches of the UPR are activated during normal differentiation of naïve B cells into plasma cells, and the Ire1 arm is essential for the expansion of their secretory network (Zhang et al., 2005; Gass et al., 2002, 2008; Iwakoshi et al., 2003; van Anken et al., 2003; Aragon et al., 2012). In contrast, the Perk arm of the UPR is dispensable for plasma cell development (Zhang et al., 2005; Gass et al., 2008). Furthermore, this pathway is suppressed during differentiation of naïve B cells into plasma cells (Ma et al., 2010; Gass et al., 2008; Zhang et al., 2005), and unrestricted Perk-eIF2α-Atf4 signaling in activated B cells blocks the formation of plasma cells (Zhu et al., 2019). Given the up-regulated expression of Atf4 in Pdap1-deficient B cells, we considered the possibility that plasma cell development might be impaired in the absence of Pdap1. To this end, we analyzed the plasma cell compartment of *Pdap1$^{F/F}$Cd19$^{Cre/+}$* mice. We found that the percentage and number of plasma cells (CD138$^+$TACI$^+$) in bone marrow and spleen of unimmunized mice was similar between control and *Pdap1$^{F/F}$Cd19$^{Cre/+}$* mice (Fig. 7 A).

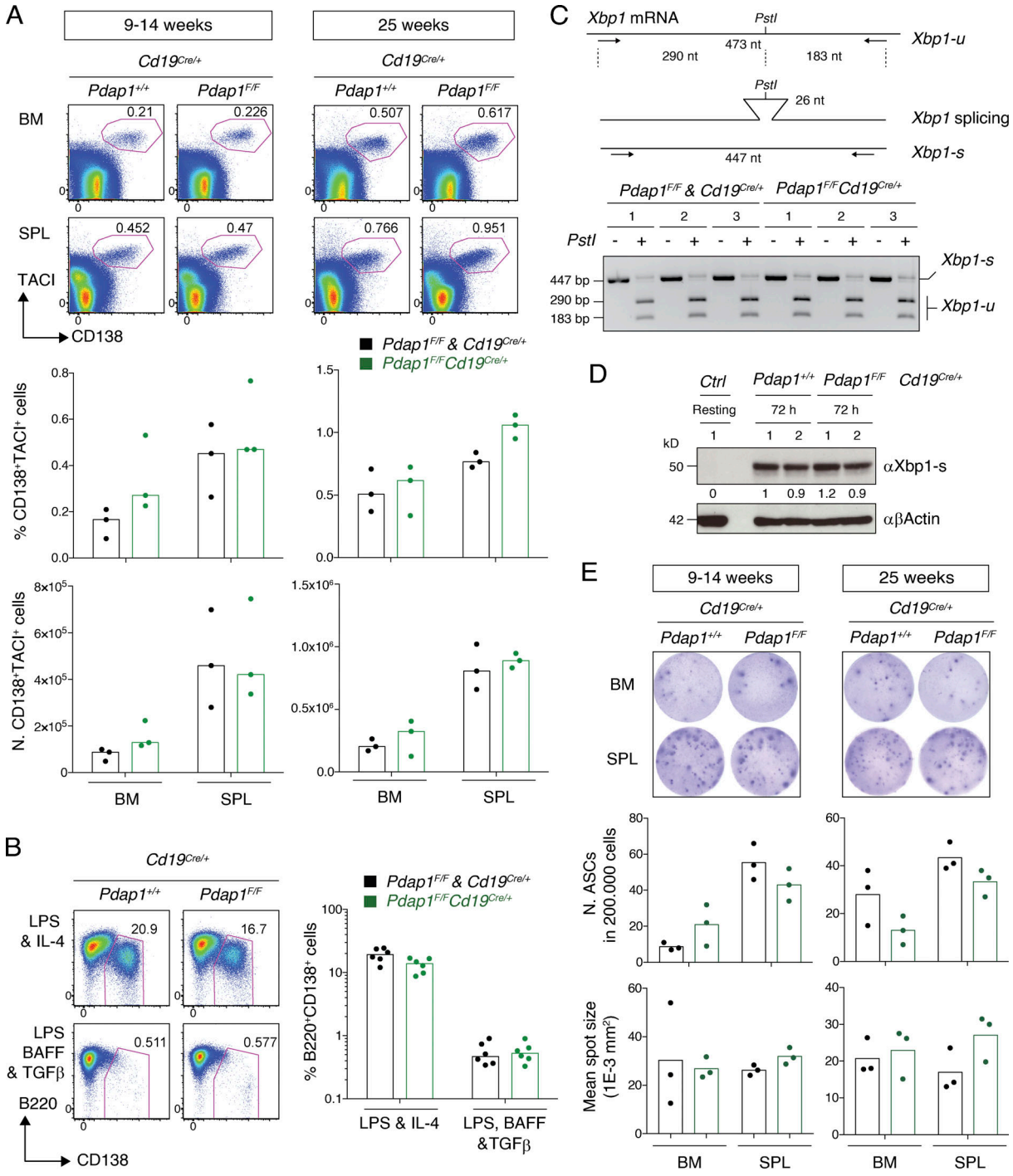

Figure 7. **Pdap1 is dispensable for plasma cell differentiation. (A)** Top: Representative flow cytometry plots showing percentage of plasma cells ($CD138^+TACI^+$) in bone marrow (BM) and spleen (SPL) of unimmunized mice of the indicated genotypes and age. Bottom: Summary graphs showing percentage and number of plasma cells for three mice per genotype and age group. N, number. **(B)** Left: Representative flow cytometry plots measuring percentage of plasmablasts ($B220^{int}CD138^+$) in splenocyte cultures of the indicated genotypes 96 h after activation with LPS and IL-4, or LPS, BAFF, and TGFβ. Right: Summary graph for six mice per genotype. **(C)** Top: Schematic representation of *Xbp1* mRNA RT-PCR and digestion products. Bottom: Electrophoretic analysis of *Xbp1* splicing in splenocytes cultures of the indicated genotypes 48 h after activation with LPS and IL-4. The DNA bands of 447 bp for the intact spliced (Xbp1-s) transcript RT-PCR product, and the unspliced (Xbp1-u) transcript digestion products of 290 and 183 bp, are indicated. Results for three mice per genotype are shown. **(D)** Representative WB analysis of splenocytes of the indicated genotypes 72 h after activation with LPS and IL-4. Resting B cells from a WT control mouse (*Ctrl*) were analyzed in parallel to show the expected undetectable levels of Xbp1-s before activation. 1 and 2 indicate two different mice per genotype. Numbers underneath the blot indicate relative quantification of Xbp1-s signal. **(E)** Top: Representative ELISpot analysis of IgM^+ ASCs in BM and SPL of unimmunized mice. Bottom: Summary graphs showing number of IgM^+ ASCs and mean surface of IgM^+ spots for three mice per genotype and age group. N, number. No difference among groups was significant for graphs in A, B, and E (Mann–Whitney *U* test).

Activation of naïve B cells with specific combinations of stimuli in vitro induces differentiation into plasmablasts. Plasmablasts are proliferating antibody-secreting cells (ASCs) whose differentiation is driven by the same transcriptional program responsible for plasma cell development (Nutt et al., 2015). Therefore, we tested the formation of plasmablasts ($B220^+CD138^+$) in vitro under the same stimulation conditions used for our previous analyses. We observed no significant difference in the percentage of plasmablasts between controls and $Pdap1^{F/F}Cd19^{Cre/+}$ cultures (Fig. 7 B). Accordingly, we did not detect any apparent change in the activation of the plasmablast and plasma cell gene signature between the two genotypes in the RNA-seq analysis (Table S1). We concluded that Atf4 up-regulation in activated $Pdap1^{F/F}Cd19^{Cre/+}$ B cells does not inhibit the generation of plasmablasts and plasma cells, and that Pdap1 is not required for the B cell developmental program controlling plasmablast and plasma cell formation and identity.

The ER expansion and increase in protein processing and folding capabilities of plasma cells are regulated by the transcription factor Xbp1-s (spliced Xbp1; Shaffer et al., 2004). Xbp1 deficiency in B cells does not interfere with the development of plasma cells but impairs immunoglobulin secretion because of defective expansion of the secretory pathway (Hu et al., 2009; Todd et al., 2009; Taubenheim et al., 2012; Shaffer et al., 2004). Xbp1-s is expressed as a result of an unconventional splicing event mediated by Ire1 that removes a 26-nt segment from *Xbp1* mRNA (unspliced *Xbp1* transcript, *Xbp1-u*), thus changing the transcript reading frame in the resulting spliced *Xbp1* transcript (*Xbp1-s*; Fig. 7 C; Yoshida et al., 2001). Xbp1-s translocates into the nucleus and activates the transcription of genes responsible for the expansion of the secretory pathway (Shaffer et al., 2004; Tellier et al., 2016). We found no difference in *Xbp1* mRNA splicing and Xbp1-s expression levels between control and $Pdap1^{F/F}Cd19^{Cre/+}$ splenocyte cultures (Fig. 7, C and D). These results suggest that the transcriptional program controlling ER network expansion in plasma cells is not affected by Pdap1 deletion. Finally, ELISpot analysis did not detect any significant difference in the number or spot size of ASCs between the two groups (Fig. 7 E), thus indicating that antibody production is not affected by Pdap1 deficiency. We concluded that Pdap1 is dispensable for the differentiation programs that establish plasma cell identity and function under steady-state conditions.

Pdap1 is required for efficient SHM of *Ig* loci

Aicda is a haploinsufficient gene, and $Aicda^{+/-}$ mice exhibit defects in both antibody diversification reactions initiated by AID, CSR, and SHM (McBride et al., 2008; Sernández et al., 2008; Takizawa et al., 2008). Given the reduced levels of AID expressed by $Pdap1^{F/F}Cd19^{Cre/+}$ B cells following activation, we considered the possibility that Pdap1 depletion might also affect SHM. To test this hypothesis, we sequenced the intronic regions downstream of the J_H4 and J_K5 elements in GC B cells sorted from Peyer's patches of aged $Pdap1^{F/F}Cd19^{Cre/+}$ mice (Jolly et al., 1997). Because of their chronic exposure to microbial antigens, GC B cells in Peyer's patches accumulate a high number of mutations over time (González-Fernández et al., 1994). Accordingly, we found that GC B cells from control mice displayed a high mutation frequency at both J_H4 and J_K5 intronic regions (Fig. 8, A–D). The vast majority of sequences contained mutations (86%, 79 of 92 for J_H4, and 83%, 104 of 125 for J_K5), and a considerable portion of B cells were heavily mutated (Fig. 8, E and F). In contrast, $Pdap1^{F/F}Cd19^{Cre/+}$ GC B cells exhibited a significantly lower mutation frequency at both J_H4 and J_K5 introns (Fig. 8, A–D). The distribution of mutations per sequence was skewed toward an increase in the proportion of sequences bearing zero or fewer than five mutations (50%, 54 of 107 for J_H4, and 65%, 83 of 127 for J_K5), whereas the number of highly mutated clones was concomitantly reduced (Fig. 8, E and F). In agreement with a role of Pdap1 in promoting AID expression rather than the processing of AID-induced lesions, the profile of mutations was not affected by Pdap1 deletion (Fig. 8, G and H).

Altogether, these findings indicate that ablation of Pdap1 impairs the efficiency of SHM of heavy and light chain *Ig* loci. Therefore, Pdap1 is required to support both antibody diversification reactions occurring in mature B cells, namely CSR and SHM.

Discussion

In this study, we report the identification of a novel factor required for mature B cell homeostasis and function. Pdap1-deficient B cells develop normally but display reduced cell viability at the mature stage both in vitro and in vivo. Furthermore, they fail to efficiently induce AID expression and cannot support physiological levels of CSR and SHM.

Pdap1 deficiency in mature B cells phenocopies key aspects of the cellular response to chronic stress. Stress-induced eIF2α phosphorylation drives the inhibition of global protein synthesis, while allowing the preferential translation of stress-responsive genes like Atf4 (Harding et al., 2000; Hinnebusch, 2000; Scheuner et al., 2001; Lu et al., 2004). The transcriptional program induced by Atf4 comprises cytoprotective genes as well as the up-regulation of biosynthetic pathways to reprogram cellular metabolism and aid homeostasis recovery. This anabolic program encompasses metabolic pathways of amino acid biosynthesis and the expression of amino acid transporter and aminoacyl-tRNA synthetase genes, and supports recovery of translation under conditions of acute stress (Harding et al., 2003; Rendleman et al., 2018; Quirós et al., 2017; Krokowski et al., 2013; Han et al., 2013). However, during chronic stress, Atf4-dependent increase in protein synthesis leads to proteotoxicity, oxidative stress, and cell death (Han et al., 2013; Krokowski et al., 2013). Pdap1-deficient B cells express Atf4 and exhibit the same transcriptional signature of Atf4-mediated translational recovery (Fig. 5, Fig. S5, and Table S1). Furthermore, the expression of this anabolic program correlates with increased apoptosis of $Pdap1^{F/F}Cd19^{Cre/+}$ B cells. Therefore, our data are consistent with a model in which ablation of Pdap1 in activated B cells leads to cell death via induction of an Atf4-dependent chronic stress response. In addition, resting B cells from Pdap1-deficient mice displayed phosphorylation of Perk and its downstream target eIF2α as well as Atf4 expression, thus indicating constitutive activation of the Perk-mediated ISR

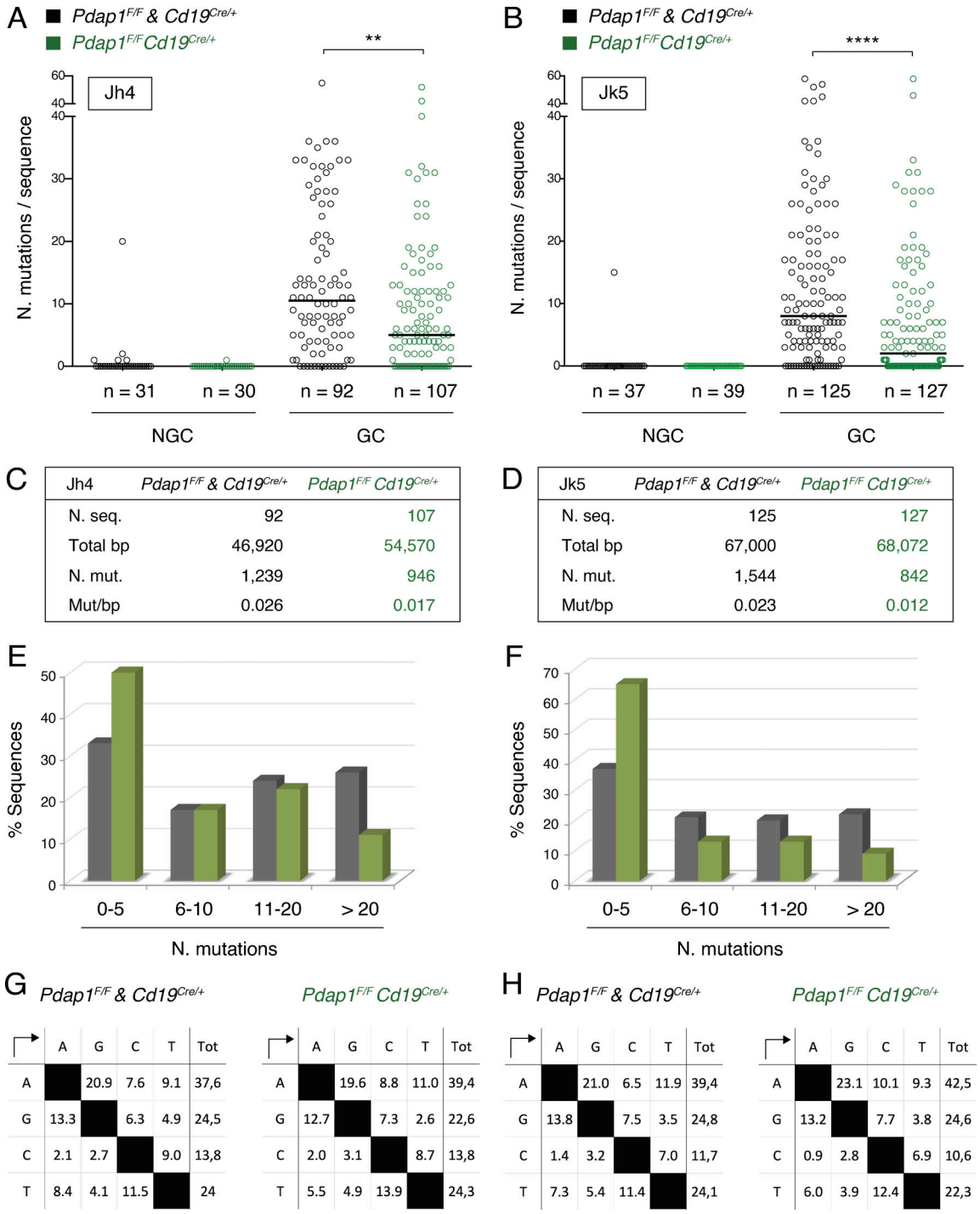

Figure 8. **Pdap1 is required for efficient SHM of *Ig* loci. (A and B)** Graphs summarizing number of mutations in 3′ J_H4 (A) and 3′ J_k5 (B) regions cloned from sorted Peyer's patches B cells of aged, unimmunized mice (five mice per genotype). Each symbol in the graphs indicates a single sequence, and the total number of sequences analyzed for each group is indicated below. Mutations were quantified for 510-bp downstream J_H4 gene segment (A) and 536-bp downstream J_K5 gene segment (B). NGC, non–GC. **(C and D)** Summary tables listing number of analyzed sequences and total length, number of mutations, and mutation frequency at J_H4 (C) and J_K5 (D) introns from A and B. **(E and F)** Graphs showing the percentage of sequences from A and B bearing the indicated mutations in 3′ J_H4 (E) and 3′ J_k5 (F). **(G and H)** Profiles of nucleotide substitutions at 3′ J_H4 (G) and 3′ J_k5 (H) regions. Significance in A and B was calculated with the Mann–Whitney *U* test, and the median is indicated. **, P ≤ 0.01; ****, P ≤ 0.0001.

pathway. This result is in agreement with the reduced number of resting B cells isolated from spleens of *Pdap1*$^{F/F}$*Cd19*$^{Cre/+}$ (Fig. S1 E) and indicates that Pdap1 deficiency is also detrimental in naïve B cells. Therefore, Pdap1 is required to protect B lymphocytes from stress-induced cell death under both resting and activated conditions.

Interestingly, while Atf4 expression increased steadily over time after activation in Pdap1-deficient B cells, phosphorylation

of Perk and eIF2α was no longer detectable. This observation has two important implications. First, the up-regulation of Atf4 expression in Pdap1-ablated cells is uncoupled from Perk-eIF2α phosphorylation following activation. This result is in agreement with the identification of a phospho-eIF2α–independent regulation of Atf4 expression observed during conditions of prolonged cellular stress (Guan et al., 2014). This regulation is likely under the control of mTORC1, which is activated in B cells after stimulation (Powell et al., 2012; Limon and Fruman, 2012; Iwata et al., 2017), and has been shown to promote Atf4 translation in a phospho-eIF2α–independent manner in other cellular contexts (Park et al., 2017; Ben-Sahra et al., 2016). Second, the dephosphorylation of Perk and eIF2α occurs at early time points after activation. This observation implies the existence of an active mechanism operating immediately upon B cell activation that physiologically inhibits the Perk-eIF2α signaling cascade. In line with this point, although mature B cells retain the potential to activate all three arms of the UPR in response to pharmacological triggers of the pathway, the Perk branch is suppressed during normal differentiation of activated B cells into plasma cells (Ma et al., 2010; Gass et al., 2008; Zhang et al., 2005). Moreover, nonphysiological Perk-eIF2α-Atf4 signaling after B cell activation even blocks the formation of plasma cells (Zhu et al., 2019). In $Pdap1^{F/F}Cd19^{Cre/+}$ splenocytes, the Perk-eIF2α-Atf4 pathway is already active under resting conditions, and the increased loss of mitochondrial membrane potential and apoptosis were observed at early, but not late, stages after activation. The earlier kinetics of Atf4 induction in our experimental conditions would explain why Pdap1 deficiency leads to cell death of naïve and early activated B cells but does not affect the plasma cell compartment. It is important to note that the analysis of plasma cell differentiation and function was performed under steady-state conditions; therefore, we cannot completely exclude the possibility that Pdap1 deficiency might affect plasma cell differentiation following immunization.

The activation of the Atf4-dependent stress response in $Pdap1^{F/F}Cd19^{Cre/+}$ B cells was accompanied by down-regulation of key factors driving antibody diversification, including AID (Muramatsu et al., 2000; Revy et al., 2000) and the transcription factor Batf, which has been shown to directly control AID expression and other aspects of the CSR program (Ise et al., 2011). Defective induction of *Aicda* expression in activated Pdap1-deficient B cells was common to all stimulation conditions (Figs. 3 A and 5 C) and likely represents the dominant cause for the reduced CSR and SHM efficiency. *Aicda* is an haploinsufficient gene, and the efficiency of CSR is directly proportional to AID levels. Mice heterozygous for a null *Aicda* allele display defects in both CSR and SHM (McBride et al., 2008; Sernández et al., 2008; Takizawa et al., 2008). Analogously, Pdap1 deficiency reduced *Aicda* expression to approximately half of WT levels in activated B cells and is associated with a similar reduction in the efficiency of both antibody diversification reactions. Furthermore, overexpression of AID in LPS-BAFF-TGFβ–stimulated splenocytes, which did not exhibit any additional defect in GLT, rescued the IgG2b CSR defect of $Pdap1^{F/F}Cd19^{Cre/+}$ B cells to a considerable extent.

Pdap1 might control activation of the ISR and the antibody diversification program via independent mechanisms. We found that Pdap1 is localized primarily in the cytoplasm in different cell types. Considering this observation and that Pdap1 was recently described as a RNA-binding protein (Castello et al., 2012, 2016; Iadevaia et al., 2020; Trendel et al., 2019; Baltz et al., 2012), it is tempting to hypothesize that it might play a role in mRNA turnover. In regard to AID, however, we showed that Pdap1 promotes its efficient expression but is dispensable for *Aicda* transcript stability. Therefore, a potential involvement of Pdap1 in the regulation of AID levels via control of mRNA turnover would occur indirectly, e.g., via modulation of the expression of intermediate factors. Although we cannot exclude the possibility that Pdap1 might regulate the expression of AID independently from its protective role against chronic ISR activation, we favor the hypothesis that the two processes are tightly linked. It is intriguing to speculate that the sustained induction of the ISR in $Pdap1^{F/F}Cd19^{Cre/+}$ B cells might actively interfere with the CSR and SHM programs. In this respect, limiting AID expression under conditions of cellular stress might represent a mechanism to alleviate the additional burden imposed by AID-induced genotoxic stress on activated B cells. Analysis of humoral responses upon genetic deletion of ISR components on a Pdap1-deficient background would provide the basis for a new exciting line of investigation into the relationship between response to cellular stresses and antibody gene diversification in mature B cells.

Materials and methods

Mouse strains

$Cd19^{Cre}$ ($Cd19^{tm1(cre)Cgn}$; Rickert et al., 1997) and $Aicda^{-/-}$ ($Aicda^{tm1Hon/tm1Hon}$; Muramatsu et al., 2000) mice were previously described and were maintained on a C57BL/6 background. The conditional $Pdap1^{F}$ allele bears LoxP sites flanking Exon 2 (ENSMUST00000031627.8) and was generated by CRISPR-Cas9–mediated knock-in microinjection of single-cell embryos on a C57BL/6N strain background (Max Delbrück Center [MDC] Transgenics platform). Germline transmission was confirmed, and positive pups were bred with $Cd19^{Cre}$ mice to generate $Pdap1^{F/F}Cd19^{Cre/+}$ mice. Mice were maintained in a specific pathogen-free barrier facility under standardized conditions (20°C ± 2°C; 55 ± 15% humidity) on a 12-h light/dark cycle. 7–27-wk-old mice of both genders were used in age-matched groups for the experiments. Controls included littermates and mice from inbred strains. All experiments were performed in compliance with European Union directive 2010/63/EU and in agreement with Landesamt für Gesundheit und Soziales directives (Berlin, Germany). Primers used for genotyping the $Pdap1^{F}$ allele are listed in Table S2.

Primary cell cultures

B lymphocytes were isolated from mouse spleens using anti-CD43 MicroBeads (Miltenyi Biotec) and grown in RPMI 1640 (Life Technologies) supplemented with 10% FBS, 10 mM Hepes (Life Technologies), 1 mM sodium pyruvate (Life Technologies), 1× Antibiotic Antimycotic (Life Technologies), 2 mM L-glutamine

(Life Technologies), and 1× 2-mercaptoethanol (Life Technologies) at 37°C and 5% CO_2.

Cell lines

The cell lines used for this study were CH12 (CH12F3, mouse; Nakamura et al., 1996); WT (R1 and R2) and Pdap1-deficient (P1, P2, and P3) CH12 clonal derivatives (mouse; this paper); BOSC23 (human; Pear et al., 1993); and immortalized mouse embryonic fibroblasts (iMEFs; Bothmer et al., 2011). CH12 cells were grown in RPMI 1640 supplemented with 10% FBS, 10 mM Hepes, 1 mM sodium pyruvate, 1× Antibiotic Antimycotic, 2 mM L-glutamine, and 1× 2-mercaptoethanol at 37°C and 5% CO_2. BOSC23 cells and iMEFs were cultured in DMEM (Life Technologies) supplemented with 10% FBS, 2 mM L-glutamine, and penicillin-streptomycin (Life Technologies) at 37°C and 5% CO_2.

CSR assay

CH12 cells were stimulated to undergo CSR to IgA by treatment with 1–5 µg/ml αCD40 (BioLegend), 5 ng/ml TGFβ (R&D Systems), and 5 ng/ml mouse recombinant IL-4 for 48 h. B lymphocytes were stimulated to undergo class switching with 5 µg/ml LPS (Sigma-Aldrich) and 5 ng/ml mouse recombinant IL-4 (Sigma-Aldrich) for CSR to IgG1; 5 µg/ml LPS only for CSR to IgG3; 5 µg/ml LPS, 10 ng/ml BAFF (PeproTech), and 2 ng/ml TGFβ for CSR to IgG2b; or 5 µg/ml LPS, 10 ng/ml BAFF, 2 ng/ml TGFβ, and 1.5 ng/ml recombinant murine IL-5 (PeproTech) for CSR to IgA. For class switching analysis, cell suspensions were stained with fluorochrome-conjugated anti-IgG1, anti-IgG3 (BD Biosciences), anti-IgG2b (BioLegend), or anti-IgA (Southern Biotech).

Retroviral infection

The pMX-AID-ER-IRES-GFP retroviral vector was a kind gift from Qiao Wang (The Rockefeller University, New York, NY). Splenocyte infections were performed as follows. The HEK293T derivative cell line BOSC23 was transfected with pCL-Eco and pMX-IRES-GFP or pMX-AID-ER-IRES-GFP retroviral vectors using FuGENE HD Transfection Reagent (Promega) to generate viral particle–containing supernatants. B cells were activated with 5 µg/ml LPS and 5 ng/ml IL-4 (IgG1) or 5 µg/ml LPS, 10 ng/ml BAFF, and 2 ng/ml TGFβ (IgG2b) and transduced twice with the viral supernatant, 1 and 2 d after isolation. 4-HT was added 72 h after activation at a final concentration of 0.05 µM, and CSR was assessed 24 h later on the GFP^+-gated populations. The pMX-Pdap1-3xFlag construct was generated by cloning the cDNA for human Pdap1 into pMX retroviral vector with a C-terminal 3xFlag tag. Primers used to clone the pMX-Pdap1-3xFlag construct are listed in Table S2. iMEFs infections were performed as indicated above for splenocytes, except that cells were transduced with pCL-Eco and pMX-EV/pMX-Pdap1-3xFlag-viral supernatants four times over 2 d. 48 h after the first transduction, iMEFs were selected using 1.5 µg/ml puromycin (Sigma-Aldrich).

B cell development and differentiation analyses

For analysis of B cell development and differentiation, spleen and bone marrow cell suspensions were incubated with ACK lysis buffer (Thermo Fisher Scientific) for erythrocyte depletion. Subsequently, cells were blocked with TruStain fcX (BioLegend) for 10 min at 4°C and labeled with fluorochrome-conjugated antibodies to determine the surface expression of CD43, IgM, CD21/CD35, and IgD (BD Biosciences), and CD23, CD3, and CD19 (BioLegend) in PBS supplemented with 3% FBS (PBS/FBS) for 20 min at 4°C. Cells were then washed, resuspended in PBS/FBS, and analyzed.

For analysis of plasma cell differentiation in vitro, splenic B cells were isolated by immunomagnetic depletion of $CD43^+$ cells and cultured at a density of 10^6 cells/ml in the presence of either 20 µg/ml LPS (Sigma-Aldrich; L2880-10MG) and 25 ng/ml IL-4, or 20 µg/ml LPS, 10 ng/ml BAFF, and 2 ng/ml TGFβ. To determine the percentage of plasmablasts, cells were harvested after 96 h, blocked with TruStain fcX for 10 min at 4°C, and stained for surface expression of B220 (BioLegend; 103245) and CD138 (BioLegend; 142506) in MACS buffer (PBS supplemented with 0.5% BSA and 2 mM EDTA) for 20 min at 4°C. Cells were then resuspended in FACS buffer (PBS supplemented with 3% FCS and 1 mM EDTA) containing 1 µg/ml propidium iodide and analyzed.

For analysis of the plasma cell compartment in vivo, 9-, 14-, and 25-wk-old mice were sacrificed to isolate the spleen and hind legs. Total splenocytes and bone marrow cells were isolated by smashing the respective organs, and erythrocytes were depleted by incubation with Gey's ABC solution for 3 min on ice. For surface staining, 5×10^6 cells were first blocked with TruStain fcX for 10 min at 4°C and then stained for the following markers for 20 min at 4°C in MACS buffer: CD138, TACI (BD PharMingen; 558410), CD93 (BioLegend; 136506), CD19 (BioLegend), and B220. Cells were resuspended in FACS buffer containing 1 µg/ml propidium iodide and analyzed.

For ELISpot analysis, $MultiScreen_{HTS}$-IP plates (Merck) were activated with 35% ethanol in PBS for 1 min, washed three times with PBS, and finally coated with 1 µg/ml anti-Igκ (Southern Biotech) and anti-Igλ (Southern Biotech) in PBS at 4°C overnight. The following day, 2×10^5 total splenocytes or BM cells (as well as serial fivefold dilutions) were cultured overnight in RPMI 1640 supplemented with 10% FCS (Sigma-Aldrich) and penicillin-streptomycin. The next day, plates were washed thoroughly six times with PBS containing 0.1% Tween20 and incubated with 1 µg/ml biotinylated antibodies against IgM (Southern Biotech) for 2 h at 37°C. Plates were washed three times under running distilled water and incubated with 0.3 U/ml streptavidin-AP (Roche) for 30 min at room temperature. For detection of spots, plates were washed three times under running distilled water, equilibrated in AP buffer (100 mM Tris-HCl, pH 9.0, 150 mM NaCl, and 1 mM $MgCl_2$), and developed using NBT/BCIP substrate mix (Promega) diluted in AP buffer. Spots were scanned and counted using the ImmunoSpot Series 6 Alfa Analyzer and ImmunoCapture Image Acquisition as well as ImmunoSpot Analysis software (C.T.L.) with the following parameters: sensitivity 176, spot separation 1.00, diffuseness largest, background balance 40, minimum spot size 0.0015 mm^2, and maximum spot size 0.6976 mm^2.

For assessment of GC B cells and CSR in vivo, cell suspensions derived from Peyer's patches were blocked with TruStain fcX for

10 min at 4°C. Subsequently, cells were stained with fluorochrome-conjugated anti-CD19, anti-B220/CD45R, anti-CD38 (BioLegend), anti-Fas/CD95, and anti-IgA (BD Biosciences) for 20 min at 4°C in PBS/FBS. Cells were washed, resuspended in PBS/FBS, and analyzed. All samples were acquired on a LSRFortessa cell analyzer (BD Biosciences).

Immunofluorescence

Resting B cells and CH12 were fixed with 4% paraformaldehyde (Sigma-Aldrich) and permeabilized with PBST (0.1% Tween 20 in PBS 1×) containing 0.2% IGEPAL CA-630 (Sigma-Aldrich). Cells were stained with antibodies against Pdap1 (Sigma-Aldrich), rat anti-mouse IgM-PE (BD Biosciences), and goat anti-rabbit Alexa Fluor 488 (Abcam). Cells were incubated with permeable nuclear dye (Hoechst dye 33258, Thermo Fisher Scientific) and transferred onto slides for imaging.

iMEFs infected with either empty pMX vector (EV) or pMX-Pdap1-3xFlag construct were grown on coverslips overnight. Upon fixation with 4% paraformaldehyde and permeabilization with 0.5% Triton X-100, cells were stained with mouse anti-Flag M2 (Sigma-Aldrich), goat anti-mouse Alexa Fluor 546 (Invitrogen), and Hoechst dye 33258. Images were acquired using inverted LSM700 AxioObserver laser scanning confocal microscope (Zeiss), with Plan-Apochromat 63×/1.40 Oil Ph3 objective for primary B cells and CH12, and EC Plan-Neofluar 40×/1.30 Oil Ph3 objective for iMEFs.

Cell proliferation and apoptosis analysis

For cell proliferation analysis by cell tracking dye dilution, primary B cells were pulsed with 5 µM CellTrace Violet (Thermo Fisher Scientific) for 10 min at 37°C. Apoptosis analysis was performed by using CaspGLOW Fluorescein Active Caspase Staining Kit (BioVision) according to the manufacturer's instructions. Samples were acquired on a LSRFortessa cell analyzer (BD Biosciences). Mitochondrial mass and membrane potential were measured via staining with MitoTracker Green and DeepRed (Thermo Fisher Scientific), respectively, according to the manufacturer's instructions. Samples were acquired on a LSRFortessa cell analyzer (BD Biosciences).

CRISPR-Cas9 gene targeting

For the loss-of-CSR assay in bulk CH12 cultures, three gRNAs against *Pdap1* gene were cloned into the U6 cassette of a variant of the original pX330 plasmid (pX330-U6-Chimeric_BB-CBh-hSpCas9, Addgene; 42230) modified to express Cas9^{WT}-T2A-GFP (kind gift from Van Trung Chu, MDC; *gPdap1-1/3*), and three gRNA pairs were cloned into tandem U6 cassettes in a mutated version of pX330 expressing Cas9^{D10A} (*Nickase-a/c*). CH12 cells were transfected with the Cas9-gRNAs expressing constructs (either individually or in a pooled format) via electroporation with Neon Transfection System (Thermo Fisher Scientific), sorted for GFP-positive cells after 40 h, and left to recover for 72 h before activation for CSR analysis. For the generation of Pdap1-deficient CH12 clonal derivatives, the *Nickases-a/c* constructs were individually electroporated into CH12. Single GFP-positive cells were sorted in 96-well plates after 40 h, and clones were allowed to grow for 12 d before CSR analysis in 96-well format and expansion of selected clones. Controls for gRNA-nucleofected CH12 were cells nucleofected with either empty vector or gRNAs against random sequences not present in the mouse genome (single random gRNA-Cas9^{WT} as controls for g*Pdap1-1/3*, and random gRNAs pairs-Cas9^{D10A} as controls for *Nickase-a/c*). Selected clones R1/R2 and P1/3 were validated at the level of genomic scar and protein expression. The sequences of the gRNAs used in these studies (this paper; Delgado-Benito et al., 2018) are listed in Table S2.

WB analysis

WB analysis of protein levels was performed on whole-cell lysates prepared by lysis in radioimmunoprecipitation assay buffer (Sigma-Aldrich) supplemented with Complete EDTA free proteinase inhibitors (Roche). Pierce Phosphatase Inhibitor Mini Tablets (Thermo Fisher Scientific) were added to the lysis buffer for the analysis of phosphorylated Perk and eIF2α. The antibodies used for WB analysis are anti-Pdap1 (Sigma-Aldrich), anti-tubulin (Abcam), anti-β-actin (Sigma), anti-AID (mAID-2; Thermo Fisher Scientific), anti-phospho-Perk (pThr980; Thermo Fisher Scientific), anti-Perk (Cell Signaling Technology), anti-phospho-eIF2α (pSer51; Cell Signaling Technology), anti-eIF2α (Santa Cruz), anti-Atf4 (Cell Signaling Technology), and anti-Xbp1-s (Cell Signaling Technology). WB signals were quantified using ImageJ (National Institutes of Health), and normalization was performed against loading controls.

qPCR

mRNA levels for AID and postspliced germline transcripts were measured as follows. Total RNA was extracted from splenocyte cultures 48 h after activation using TRIzol (Invitrogen) according to manufacturer's instructions and retro-transcribed with SuperScript VILO cDNA Synthesis Kit (Invitrogen). Genomic DNA was removed by RapidOut DNA Removal Kit (Thermo Fisher Scientific). Transcripts were amplified using StepOnePlus Real-Time PCR System (Applied Biosystems) with Luna Universal qPCR Mastermix (NEB). For analysis of *Aicda* mRNA decay, Actinomycin D was added to the culture medium 48 h after activation at a final concentration of 10 µg/ml for 0.5, 1, 1.5, 2, 3, and 4 h. qPCR analyses were normalized to *Ubc* or *Gapdh* (*Aicda* mRNA and GLTs) or *Gapdh* (*Aicda* mRNA decay). Primers used for qPCR (this paper; Xu et al., 2015; Muramatsu et al., 2000; Albershardt et al., 2012) are listed in Table S2.

For electrophoretic analysis of *Xbp1* splicing, *Xbp1* transcripts were amplified using the primers listed in Table S2 (Madaro et al., 2013) and either mock-digested or digested with PstI enzyme (NEB) for 30 min at 37°C. The intact spliced (Xbp1-s) transcript RT-PCR product and the unspliced (Xbp1-u) transcript digestion products were visualized on 2% agarose gel.

RNA-seq

RNA-seq was performed on three mice per genotype. Splenocytes were cultured in LPS and IL-4 (IgG1) or LPS, BAFF, and TGFβ (IgG2b) for 48 h. Cells were collected by centrifugation, and RNA was extracted with TRIzol (Invitrogen) according to manufacturer's instructions. Ribosomal RNA was depleted using Ribo-Zero Gold rRNA Removal Kit (Illumina). Libraries were

prepared with TruSeq Stranded Total RNA Library Prep Kit Gold (Illumina) and run in one lane of a flow cell of HiSeq 4000 (Illumina).

The RNA-seq data were analyzed using the pigx-rnaseq pipeline (Wurmus et al., 2018). STAR (Dobin et al., 2013) mapped the reads to the GRCm38 assembly for mouse by Ensembl, and HTSeq (Anders et al., 2015) was used to count the transcript abundance. Differential expression analysis was done using the DESeq2 (Love et al., 2014) package for R, which uses the Wald test for significance.

For splicing analysis of *Aicda* and *Pdap1* genes, we used the edgeR (Robinson et al., 2010) package for R to determine differentially expressed exons. The annotation was provided by a filtered version of the GRCm38 gene annotation, which contained unique, Havana-annotated exons.

SHM analysis

Single-cell suspensions from Peyer's patches of 24–27-wk-old mice were first incubated with TruStain fcX, and then labeled with antibodies conjugated with B220-FITC (BioLegend), CD19-APC/Pacific Blue (BioLegend), CD38-Alexa Fluor 700 (Thermo Fisher Scientific), and CD95/Fas-PE (BD Biosciences). Non-GC ($CD38^+$ Fas^-) and GC B cells ($CD38^-$ Fas^+) were sorted on an Aria BD sorter. Genomic DNA was extracted, and the 5′ portions of J_H4 (*Igh*) and J_K5 (*Igk*) introns were amplified by PCR using Phusion High-Fidelity DNA Polymerase (Thermo Fisher Scientific). The 800-bp J_H4 and 700-bp J_K5 PCR products were gel extracted, cloned into a pCR2.1 vector using the TOPO TA Cloning Kit (Invitrogen), and sequenced. Mutations were quantified over 510-bp downstream J_H4 and 536-bp downstream J_K5 gene segments. Primers used for SHM analysis (Rouaud et al., 2013; Sander et al., 2015) are listed in Table S2.

Seahorse assay

Oxygen consumption rate and extracellular acidification rate were measured with the Seahorse XF96 metabolite analyzer using the Seahorse XF Cell Mito Stress Test kit (Agilent). Primary B cells were isolated, counted, and plated at the indicated cell densities directly on Seahorse cell culture plates coated with poly-L-lysine (Sigma-Aldrich). Before measurement, cells were incubated for a maximum of 1 h in Seahorse XF DMEM medium pH 7.4 (Agilent) supplemented with 10 mM glucose (Agilent), 1 mM sodium pyruvate (Agilent), and 2 mM L-glutamine (Agilent).

Statistical analysis

The statistical significance of differences between groups/datasets was determined by the Mann–Whitney *U* test for all data presented in this study, with the following exceptions. For the RNA-seq analysis, the Wald test of the DESeq2 package for R was used, and we considered genes with an FDR < 0.05 to be significantly differentially expressed. Statistical details of experiments can be found in the figure legends.

Data availability

The deep-sequencing data reported in this paper (RNA-seq) has been deposited in the GEO repository under accession no. GSE141876.

Online supplemental material

Fig. S1 shows that Pdap1 is dispensable for B cell development. Fig. S2 shows that Pdap1 is dispensable for B cell proliferation. Fig. S3 shows that *Aicda* mRNA levels are reduced in Pdap1-deficient CH12 cell lines. Fig. S4 shows that Pdap1 is localized primarily in the cytoplasm in B cells and MEFs. Fig. S5 shows the stress response signature of Pdap1-deficient B cells. Table S1 contains the pairwise comparison of differentially regulated genes in control versus $Pdap1^{F/F}Cd19^{Cre/+}$ splenocytes. Table S2 lists the oligonucleotides used in this study.

Acknowledgments

We thank all members of the Di Virgilio laboratory for their feedback and discussion; V. Coralluzzo (Di Virgilio Lab, MDC, Berlin) for support with genotyping; Y. Dramaretska (Gargiulo Lab, MDC) for helpful tips on the RNA-seq protocol; the MDC Transgenics platform and Dr. R. Kühn for generation of the $Pdap1^F$ mouse allele; the MDC FACS Core Facility and Dr. H.P. Rahn for assistance with cell sorting; K. Rajewsky (MDC) for feedback and discussion; and N. Zampieri (MDC) for critical reading of the manuscript and advice.

This work was supported by the European Research Council (grant 638897 to M. Di Virgilio), the Helmholtz-Gemeinschaft Zukunftsthema "Immunology and Inflammation" (ZT-0027 to M. Di Virgilio), and the Deutsche Krebshilfe (grant 70112800 to M. Janz). M. Di Virgilio is a Helmholtz Young Investigators Group leader (Helmholtz Association).

Author contributions: M. Di Virgilio and V. Delgado-Benito conceived the project idea and designed the experiments; M. Di Virgilio, V. Delgado-Benito, and M. Berruezo-Llacuna analyzed and interpreted the data; V. Delgado-Benito, M. Berruezo-Llacuna, W. Winkler, D. Sundaravinayagam, S. Balasubramanian, M. Caganova, A. Rahjouei, M.-T. Henke, M. Driesner, and L. Keller performed the experiments; R. Altwasser performed all RNA-seq data analyses; R. Graf contributed to design of the list of gRNAs used for the initial loss-of-CSR screen; A. Prigione, M. Janz, A. Akalin, and M. Di Virgilio supervised the experiments or analyses performed in their respective groups; M. Di Virgilio obtained the funding for the project and wrote the manuscript.

Disclosures: The authors declare no competing interests exist.

Submitted: 27 January 2020
Revised: 20 April 2020
Accepted: 19 May 2020

References

Albershardt, T.C., B.M. Iritani, and A. Ruddell. 2012. Evaluation of reference genes for quantitative PCR analysis of mouse lymphocytes. *J. Immunol. Methods*. 384:196–199. https://doi.org/10.1016/j.jim.2012.07.020

Anders, S., P.T. Pyl, and W. Huber. 2015. HTSeq--a Python framework to work with high-throughput sequencing data. *Bioinformatics*. 31:166–169. https://doi.org/10.1093/bioinformatics/btu638

Aragon, I.V., R.A. Barrington, S. Jackowski, K. Mori, and J.W. Brewer. 2012. The specialized unfolded protein response of B lymphocytes: ATF6α-independent development of antibody-secreting B cells. *Mol. Immunol.* 51:347–355. https://doi.org/10.1016/j.molimm.2012.04.001

Arnold, L.W., N.J. LoCascio, P.M. Lutz, C.A. Pennell, D. Klapper, and G. Haughton. 1983. Antigen-induced lymphomagenesis: identification of a murine B cell lymphoma with known antigen specificity. *J. Immunol.* 131:2064–2068.

Baltz, A.G., M. Munschauer, B. Schwanhäusser, A. Vasile, Y. Murakawa, M. Schueler, N. Youngs, D. Penfold-Brown, K. Drew, M. Milek, et al. 2012. The mRNA-bound proteome and its global occupancy profile on protein-coding transcripts. *Mol. Cell.* 46:674–690. https://doi.org/10.1016/j.molcel.2012.05.021

Ben-Sahra, I., G. Hoxhaj, S.J.H. Ricoult, J.M. Asara, and B.D. Manning. 2016. mTORC1 induces purine synthesis through control of the mitochondrial tetrahydrofolate cycle. *Science.* 351:728–733. https://doi.org/10.1126/science.aad0489

Bishop, G.A., and G. Haughton. 1986. Induced differentiation of a transformed clone of Ly-1+ B cells by clonal T cells and antigen. *Proc. Natl. Acad. Sci. USA.* 83:7410–7414. https://doi.org/10.1073/pnas.83.19.7410

Boboila, C., F.W. Alt, and B. Schwer. 2012. Classical and Alternative End-Joining Pathways for Repair of Lymphocyte-Specific and General DNA Double-Strand Breaks. *In* Adv. Immunol. Vol. 116. pp. 1–49.

Bothmer, A., D.F. Robbiani, M. Di Virgilio, S.F. Bunting, I.A. Klein, N. Feldhahn, J. Barlow, H.T. Chen, D. Bosque, E. Callen, et al. 2011. Regulation of DNA end joining, resection, and immunoglobulin class switch recombination by 53BP1. *Mol. Cell.* 42:319–329. https://doi.org/10.1016/j.molcel.2011.03.019

Bransteitter, R., P. Pham, M.D. Scharff, and M.F. Goodman. 2003. Activation-induced cytidine deaminase deaminates deoxycytidine on single-stranded DNA but requires the action of RNase. *Proc. Natl. Acad. Sci. USA.* 100:4102–4107. https://doi.org/10.1073/pnas.0730835100

Brostrom, C.O., and M.A. Brostrom. 1998. Regulation of translational initiation during cellular responses to stress. *Prog. Nucleic Acid Res. Mol. Biol.* 58:79–125. https://doi.org/10.1016/S0079-6603(08)60034-3

Brostrom, C.O., C.R. Prostko, R.J. Kaufman, and M.A. Brostrom. 1996. Inhibition of translational initiation by activators of the glucose-regulated stress protein and heat shock protein stress response systems. Role of the interferon-inducible double-stranded RNA-activated eukaryotic initiation factor 2α kinase. *J. Biol. Chem.* 271:24995–25002. https://doi.org/10.1074/jbc.271.40.24995

Brostrom, M.A., X.J. Lin, C. Cade, D. Gmitter, and C.O. Brostrom. 1989. Loss of a calcium requirement for protein synthesis in pituitary cells following thermal or chemical stress. *J. Biol. Chem.* 264:1638–1643.

Castello, A., B. Fischer, K. Eichelbaum, R. Horos, B.M. Beckmann, C. Strein, N.E. Davey, D.T. Humphreys, T. Preiss, L.M. Steinmetz, et al. 2012. Insights into RNA biology from an atlas of mammalian mRNA-binding proteins. *Cell.* 149:1393–1406. https://doi.org/10.1016/j.cell.2012.04.031

Castello, A., B. Fischer, C.K. Frese, R. Horos, A.M. Alleaume, S. Foehr, T. Curk, J. Krijgsveld, and M.W. Hentze. 2016. Comprehensive Identification of RNA-Binding Domains in Human Cells. *Mol. Cell.* 63:696–710. https://doi.org/10.1016/j.molcel.2016.06.029

Cattoretti, G., M. Büttner, R. Shaknovich, E. Kremmer, B. Alobeid, and G. Niedobitek. 2006. Nuclear and cytoplasmic AID in extrafollicular and germinal center B cells. *Blood.* 107:3967–3975. https://doi.org/10.1182/blood-2005-10-4170

Chaudhuri, J., M. Tian, C. Khuong, K. Chua, E. Pinaud, and F.W. Alt. 2003. Transcription-targeted DNA deamination by the AID antibody diversification enzyme. *Nature.* 422:726–730. https://doi.org/10.1038/nature01574

Corley, R.B., N.J. LoCascio, M. Ovnic, and G. Haughton. 1985. Two separate functions of class II (Ia) molecules: T-cell stimulation and B-cell excitation. *Proc. Natl. Acad. Sci. USA.* 82:516–520. https://doi.org/10.1073/pnas.82.2.516

Crouch, E.E., Z. Li, M. Takizawa, S. Fichtner-Feigl, P. Gourzi, C. Montaño, L. Feigenbaum, P. Wilson, S. Janz, F.N. Papavasiliou, et al. 2007. Regulation of AID expression in the immune response. *J. Exp. Med.* 204:1145–1156. https://doi.org/10.1084/jem.20061952

Cunningham, A.F., K. Serre, E. Mohr, M. Khan, and K.M. Toellner. 2004. Loss of CD154 impairs the Th2 extrafollicular plasma cell response but not early T cell proliferation and interleukin-4 induction. *Immunology.* 113:187–193. https://doi.org/10.1111/j.1365-2567.2004.01951.x

Cyster, J.G., and C.D.C. Allen. 2019. B Cell Responses: Cell Interaction Dynamics and Decisions. *Cell.* 177:524–540. https://doi.org/10.1016/j.cell.2019.03.016

Dedeoglu, F., B. Horwitz, J. Chaudhuri, F.W. Alt, and R.S. Geha. 2004. Induction of activation-induced cytidine deaminase gene expression by IL-4 and CD40 ligation is dependent on STAT6 and NFkappaB. *Int. Immunol.* 16:395–404. https://doi.org/10.1093/intimm/dxh042

Deenick, E.K., J. Hasbold, and P.D. Hodgkin. 1999. Switching to IgG3, IgG2b, and IgA is division linked and independent, revealing a stochastic framework for describing differentiation. *J. Immunol.* 163:4707–4714.

Delgado-Benito, V., D.B. Rosen, Q. Wang, A. Gazumyan, J.A. Pai, T.Y. Oliveira, D. Sundaravinayagam, W. Zhang, M. Andreani, L. Keller, et al. 2018. The Chromatin Reader ZMYND8 Regulates Igh Enhancers to Promote Immunoglobulin Class Switch Recombination. *Mol. Cell.* 72:636–649.e8. https://doi.org/10.1016/j.molcel.2018.08.042

Dever, T.E., L. Feng, R.C. Wek, A.M. Cigan, T.F. Donahue, and A.G. Hinnebusch. 1992. Phosphorylation of initiation factor 2 α by protein kinase GCN2 mediates gene-specific translational control of GCN4 in yeast. *Cell.* 68:585–596. https://doi.org/10.1016/0092-8674(92)90193-G

Dickerson, S.K., E. Market, E. Besmer, and F.N. Papavasiliou. 2003. AID mediates hypermutation by deaminating single stranded DNA. *J. Exp. Med.* 197:1291–1296. https://doi.org/10.1084/jem.20030481

Dobin, A., C.A. Davis, F. Schlesinger, J. Drenkow, C. Zaleski, S. Jha, P. Batut, M. Chaisson, and T.R. Gingeras. 2013. STAR: ultrafast universal RNA-seq aligner. *Bioinformatics.* 29:15–21. https://doi.org/10.1093/bioinformatics/bts635

Donnelly, N., A.M. Gorman, S. Gupta, and A. Samali. 2013. The eIF2α kinases: their structures and functions. *Cell. Mol. Life Sci.* 70:3493–3511. https://doi.org/10.1007/s00018-012-1252-6

Dorsett, Y., K.M. McBride, M. Jankovic, A. Gazumyan, T.H. Thai, D.F. Robbiani, M. Di Virgilio, B. Reina San-Martin, G. Heidkamp, T.A. Schwickert, et al. 2008. MicroRNA-155 suppresses activation-induced cytidine deaminase-mediated Myc-Igh translocation. *Immunity.* 28:630–638. https://doi.org/10.1016/j.immuni.2008.04.002

Dudley, D.D., J. Chaudhuri, C.H. Bassing, and F.W. Alt. 2005. Mechanism and control of V(D)J recombination versus class switch recombination: similarities and differences. *Adv. Immunol.* 86:43–112. https://doi.org/10.1016/S0065-2776(04)86002-4

Dufort, F.J., M.R. Gumina, N.L. Ta, Y. Tao, S.A. Heyse, D.A. Scott, A.D. Richardson, T.N. Seyfried, and T.C. Chiles. 2014. Glucose-dependent de novo lipogenesis in B lymphocytes: a requirement for atp-citrate lyase in lipopolysaccharide-induced differentiation. *J. Biol. Chem.* 289:7011–7024. https://doi.org/10.1074/jbc.M114.551051

Durandy, A., S. Kracker, and A. Fischer. 2013. Primary antibody deficiencies. *Nat. Rev. Immunol.* 13:519–533. https://doi.org/10.1038/nri3466

Fagone, P., R. Sriburi, C. Ward-Chapman, M. Frank, J. Wang, C. Gunter, J.W. Brewer, and S. Jackowski. 2007. Phospholipid biosynthesis program underlying membrane expansion during B-lymphocyte differentiation. *J. Biol. Chem.* 282:7591–7605. https://doi.org/10.1074/jbc.M608175200

Fischer, W.H., and D. Schubert. 1996. Characterization of a novel platelet-derived growth factor-associated protein. *J. Neurochem.* 66:2213–2216. https://doi.org/10.1046/j.1471-4159.1996.66052213.x

Gass, J.N., N.M. Gifford, and J.W. Brewer. 2002. Activation of an unfolded protein response during differentiation of antibody-secreting B cells. *J. Biol. Chem.* 277:49047–49054. https://doi.org/10.1074/jbc.M205011200

Gass, J.N., H.Y. Jiang, R.C. Wek, and J.W. Brewer. 2008. The unfolded protein response of B-lymphocytes: PERK-independent development of antibody-secreting cells. *Mol. Immunol.* 45:1035–1043. https://doi.org/10.1016/j.molimm.2007.07.029

Gonda, H., M. Sugai, Y. Nambu, T. Katakai, Y. Agata, K.J. Mori, Y. Yokota, and A. Shimizu. 2003. The balance between Pax5 and Id2 activities is the key to AID gene expression. *J. Exp. Med.* 198:1427–1437. https://doi.org/10.1084/jem.20030802

González-Fernández, A., D. Gilmore, and C. Milstein. 1994. Age-related decrease in the proportion of germinal center B cells from mouse Peyer's patches is accompanied by an accumulation of somatic mutations in their immunoglobulin genes. *Eur. J. Immunol.* 24:2918–2921. https://doi.org/10.1002/eji.1830241151

Gottlieb, E., S.M. Armour, M.H. Harris, and C.B. Thompson. 2003. Mitochondrial membrane potential regulates matrix configuration and cytochrome c release during apoptosis. *Cell Death Differ.* 10:709–717. https://doi.org/10.1038/sj.cdd.4401231

Guan, B.J., D. Krokowski, M. Majumder, C.L. Schmotzer, S.R. Kimball, W.C. Merrick, A.E. Koromilas, and M. Hatzoglou. 2014. Translational control during endoplasmic reticulum stress beyond phosphorylation of the translation initiation factor eIF2α. *J. Biol. Chem.* 289:12593–12611. https://doi.org/10.1074/jbc.M113.543215

Gupta, S., D.E. Read, A. Deepti, K. Cawley, A. Gupta, D. Oommen, T. Verfaillie, S. Matus, M.A. Smith, J.L. Mott, et al. 2012. Perk-dependent repression of miR-106b-25 cluster is required for ER stress-induced apoptosis. *Cell Death Dis.* 3. e333. https://doi.org/10.1038/cddis.2012.74

Han, J., S.H. Back, J. Hur, Y.H. Lin, R. Gildersleeve, J. Shan, C.L. Yuan, D. Krokowski, S. Wang, M. Hatzoglou, et al. 2013. ER-stress-induced transcriptional regulation increases protein synthesis leading to cell death. *Nat. Cell Biol.* 15:481–490. https://doi.org/10.1038/ncb2738

Harding, H.P., I. Novoa, Y. Zhang, H. Zeng, R. Wek, M. Schapira, and D. Ron. 2000. Regulated translation initiation controls stress-induced gene expression in mammalian cells. *Mol. Cell.* 6:1099–1108. https://doi.org/10.1016/S1097-2765(00)00108-8

Harding, H.P., Y. Zhang, and D. Ron. 1999. Protein translation and folding are coupled by an endoplasmic-reticulum-resident kinase. *Nature*. 397: 271–274. https://doi.org/10.1038/16729

Harding, H.P., Y. Zhang, H. Zeng, I. Novoa, P.D. Lu, M. Calfon, N. Sadri, C. Yun, B. Popko, R. Paules, et al. 2003. An integrated stress response regulates amino acid metabolism and resistance to oxidative stress. *Mol. Cell.* 11:619–633. https://doi.org/10.1016/S1097-2765(03)00105-9

Hasbold, J., J.S.-Y. Hong, M.R. Kehry, and P.D. Hodgkin. 1999. Integrating signals from IFN-gamma and IL-4 by B cells: positive and negative effects on CD40 ligand-induced proliferation, survival, and division-linked isotype switching to IgG1, IgE, and IgG2a. *J. Immunol.* 163: 4175–4181.

Hasbold, J., A.B. Lyons, M.R. Kehry, and P.D. Hodgkin. 1998. Cell division number regulates IgG1 and IgE switching of B cells following stimulation by CD40 ligand and IL-4. *Eur. J. Immunol.* 28:1040–1051. https://doi.org/10.1002/(SICI)1521-4141(199803)28:03<1040::AID-IMMU1040>3.0.CO;2-9

Haze, K., T. Okada, H. Yoshida, H. Yanagi, T. Yura, M. Negishi, and K. Mori. 2001. Identification of the G13 (cAMP-response-element-binding protein-related protein) gene product related to activating transcription factor 6 as a transcriptional activator of the mammalian unfolded protein response. *Biochem. J.* 355:19–28. https://doi.org/10.1042/bj3550019

Haze, K., H. Yoshida, H. Yanagi, T. Yura, and K. Mori. 1999. Mammalian transcription factor ATF6 is synthesized as a transmembrane protein and activated by proteolysis in response to endoplasmic reticulum stress. *Mol. Biol. Cell.* 10:3787–3799. https://doi.org/10.1091/mbc.10.11.3787

Hinnebusch, A.G.. 2000. Mechanism and Regulation of Initiator Methionyl-tRNA Binding to Ribosomes. *In* Translational Control of Gene Expression. N. Sonenberg, J.W.B. Hershey, and M.B. Mathews, editors. CSHL Press, Cold Spring Harbor, NY. pp. 185–243.

Hiramatsu, N., C. Messah, J. Han, M.M. LaVail, R.J. Kaufman, and J.H. Lin. 2014. Translational and posttranslational regulation of XIAP by eIF2α and ATF4 promotes ER stress-induced cell death during the unfolded protein response. *Mol. Biol. Cell.* 25:1411–1420. https://doi.org/10.1091/mbc.e13-11-0664

Hodgkin, P.D., J.H. Lee, and A.B. Lyons. 1996. B cell differentiation and isotype switching is related to division cycle number. *J. Exp. Med.* 184: 277–281. https://doi.org/10.1084/jem.184.1.277

Hu, C.C.A., S.K. Dougan, A.M. McGehee, J.C. Love, and H.L. Ploegh. 2009. XBP-1 regulates signal transduction, transcription factors and bone marrow colonization in B cells. *EMBO J.* 28:1624–1636. https://doi.org/10.1038/emboj.2009.117

Iadevaia, V., M.D. Wouters, A. Kanitz, A.M. Matia-González, E.E. Laing, and A.P. Gerber. 2020. Tandem RNA isolation reveals functional rearrangement of RNA-binding proteins on *CDKN1B/p27*^{Kip1} 3'UTRs in cisplatin treated cells. *RNA Biol.* 17:33–46. https://doi.org/10.1080/15476286.2019.1662268

Ise, W., M. Kohyama, B.U. Schraml, T. Zhang, B. Schwer, U. Basu, F.W. Alt, J. Tang, E.M. Oltz, T.L. Murphy, et al. 2011. The transcription factor BATF controls the global regulators of class-switch recombination in both B cells and T cells. *Nat. Immunol.* 12:536–543. https://doi.org/10.1038/ni.2037

Iwakoshi, N.N., A.H. Lee, P. Vallabhajosyula, K.L. Otipoby, K. Rajewsky, and L.H. Glimcher. 2003. Plasma cell differentiation and the unfolded protein response intersect at the transcription factor XBP-1. *Nat. Immunol.* 4:321–329. https://doi.org/10.1038/ni907

Iwata, T.N., J.A. Ramírez-Komo, H. Park, and B.M. Iritani. 2017. Control of B lymphocyte development and functions by the mTOR signaling pathways. *Cytokine Growth Factor Rev.* 35:47–62. https://doi.org/10.1016/j.cytogfr.2017.04.005

Jolly, C.J., N. Klix, and M.S. Neuberger. 1997. Rapid methods for the analysis of immunoglobulin gene hypermutation: application to transgenic and gene targeted mice. *Nucleic Acids Res.* 25:1913–1919. https://doi.org/10.1093/nar/25.10.1913

Kojima, E., A. Takeuchi, M. Haneda, A. Yagi, T. Hasegawa, K. Yamaki, K. Takeda, S. Akira, K. Shimokata, and K. Isobe. 2003. The function of GADD34 is a recovery from a shutoff of protein synthesis induced by ER stress: elucidation by GADD34-deficient mice. *FASEB J.* 17:1573–1575. https://doi.org/10.1096/fj.02-1184fje

Krokowski, D., J. Han, M. Saikia, M. Majumder, C.L. Yuan, B.J. Guan, E. Bevilacqua, O. Bussolati, S. Bröer, P. Arvan, et al. 2013. A self-defeating anabolic program leads to β-cell apoptosis in endoplasmic reticulum stress-induced diabetes via regulation of amino acid flux. *J. Biol. Chem.* 288:17202–17213. https://doi.org/10.1074/jbc.M113.466920

Limon, J.J., and D.A. Fruman. 2012. Akt and mTOR in B cell activation and differentiation. *Front. Immunol.* 3:228. https://doi.org/10.3389/fimmu.2012.00228

LoCascio, N.J., L.W. Arnold, R.B. Corley, and G. Haughton. 1984a. Induced differentiation of a B cell lymphoma with known antigen specificity. *J. Mol. Cell. Immunol.* 1:177–190.

LoCascio, N.J., G. Haughton, L.W. Arnold, and R.B. Corley. 1984b. Role of cell surface immunoglobulin in B-lymphocyte activation. *Proc. Natl. Acad. Sci. USA.* 81:2466–2469. https://doi.org/10.1073/pnas.81.8.2466

Love, M.I., W. Huber, and S. Anders. 2014. Moderated estimation of fold change and dispersion for RNA-seq data with DESeq2. *Genome Biol.* 15: 550. https://doi.org/10.1186/s13059-014-0550-8

Lu, P.D., H.P. Harding, and D. Ron. 2004. Translation reinitiation at alternative open reading frames regulates gene expression in an integrated stress response. *J. Cell Biol.* 167:27–33. https://doi.org/10.1083/jcb.200408003

Ma, Y., and L.M. Hendershot. 2003. Delineation of a negative feedback regulatory loop that controls protein translation during endoplasmic reticulum stress. *J. Biol. Chem.* 278:34864–34873. https://doi.org/10.1074/jbc.M301107200

Ma, Y., Y. Shimizu, M.J. Mann, Y. Jin, and L.M. Hendershot. 2010. Plasma cell differentiation initiates a limited ER stress response by specifically suppressing the PERK-dependent branch of the unfolded protein response. *Cell Stress Chaperones.* 15:281–293. https://doi.org/10.1007/s12192-009-0142-9

Madaro, L., V. Marrocco, S. Carnio, M. Sandri, and M. Bouché. 2013. Intracellular signaling in ER stress-induced autophagy in skeletal muscle cells. *FASEB J.* 27:1990–2000. https://doi.org/10.1096/fj.12-215475

Marciniak, S.J., C.Y. Yun, S. Oyadomari, I. Novoa, Y. Zhang, R. Jungreis, K. Nagata, H.P. Harding, and D. Ron. 2004. CHOP induces death by promoting protein synthesis and oxidation in the stressed endoplasmic reticulum. *Genes Dev.* 18:3066–3077. https://doi.org/10.1101/gad.1250704

Matthews, A.J., S. Zheng, L.J. DiMenna, and J. Chaudhuri. 2014. Regulation of Immunoglobulin Class-Switch Recombination: Choreography of Noncoding Transcription, Targeted DNA Deamination, and Long-Range DNA Repair. *In* Adv. Immunol. Vol. 122. pp. 1–57.

McBride, K.M., A. Gazumyan, E.M. Woo, T.A. Schwickert, B.T. Chait, and M.C. Nussenzweig. 2008. Regulation of class switch recombination and somatic mutation by AID phosphorylation. *J. Exp. Med.* 205:2585–2594. https://doi.org/10.1084/jem.20081319

Methot, S.P., and J.M. Di Noia. 2017. Molecular Mechanisms of Somatic Hypermutation and Class Switch Recombination. *Adv. Immunol.* 133:37–87. https://doi.org/10.1016/bs.ai.2016.11.002

Minnich, M., H. Tagoh, P. Bönelt, E. Axelsson, M. Fischer, B. Cebolla, A. Tarakhovsky, S.L. Nutt, M. Jaritz, and M. Busslinger. 2016. Multifunctional role of the transcription factor Blimp-1 in coordinating plasma cell differentiation. *Nat. Immunol.* 17:331–343. https://doi.org/10.1038/ni.3349

Muramatsu, M., K. Kinoshita, S. Fagarasan, S. Yamada, Y. Shinkai, and T. Honjo. 2000. Class switch recombination and hypermutation require activation-induced cytidine deaminase (AID), a potential RNA editing enzyme. *Cell.* 102:553–563. https://doi.org/10.1016/S0092-8674(00)00078-7

Muramatsu, M., V.S. Sankaranand, S. Anant, M. Sugai, K. Kinoshita, N.O. Davidson, and T. Honjo. 1999. Specific expression of activation-induced cytidine deaminase (AID), a novel member of the RNA-editing deaminase family in germinal center B cells. *J. Biol. Chem.* 274:18470–18476. https://doi.org/10.1074/jbc.274.26.18470

Nakamura, M., S. Kondo, M. Sugai, M. Nazarea, S. Imamura, and T. Honjo. 1996. High frequency class switching of an IgM+ B lymphoma clone CH12F3 to IgA+ cells. *Int. Immunol.* 8:193–201. https://doi.org/10.1093/intimm/8.2.193

Novoa, I., Y. Zhang, H. Zeng, R. Jungreis, H.P. Harding, and D. Ron. 2003. Stress-induced gene expression requires programmed recovery from translational repression. *EMBO J.* 22:1180–1187. https://doi.org/10.1093/emboj/cdg112

Nutt, S.L., P.D. Hodgkin, D.M. Tarlinton, and L.M. Corcoran. 2015. The generation of antibody-secreting plasma cells. *Nat. Rev. Immunol.* 15: 160–171. https://doi.org/10.1038/nri3795

Ohoka, N., S. Yoshii, T. Hattori, K. Onozaki, and H. Hayashi. 2005. TRB3, a novel ER stress-inducible gene, is induced via ATF4-CHOP pathway and is involved in cell death. *EMBO J.* 24:1243–1255. https://doi.org/10.1038/sj.emboj.7600596

Ovnic, M., and R.B. Corley. 1987. Quantitation of cell surface molecules on a differentiating, Ly-1+ B cell lymphoma. *J. Immunol.* 138:3075–3082.

Pakos-Zebrucka, K., I. Koryga, K. Mnich, M. Ljujic, A. Samali, and A.M. Gorman. 2016. The integrated stress response. *EMBO Rep.* 17:1374–1395. https://doi.org/10.15252/embr.201642195

Park, Y., A. Reyna-Neyra, L. Philippe, and C.C. Thoreen. 2017. mTORC1 Balances Cellular Amino Acid Supply with Demand for Protein Synthesis through Post-transcriptional Control of ATF4. *Cell Rep.* 19:1083–1090. https://doi.org/10.1016/j.celrep.2017.04.042

Pavri, R., and M.C. Nussenzweig. 2011. AID targeting in antibody diversity. *Adv. Immunol.* 110:1–26. https://doi.org/10.1016/B978-0-12-387663-8.00005-3

Pear, W.S., G.P. Nolan, M.L. Scott, and D. Baltimore. 1993. Production of high-titer helper-free retroviruses by transient transfection. *Proc. Natl. Acad. Sci. USA.* 90:8392–8396. https://doi.org/10.1073/pnas.90.18.8392

Peled, J.U., F.L. Kuang, M.D. Iglesias-Ussel, S. Roa, S.L. Kalis, M.F. Goodman, and M.D. Scharff. 2008. The biochemistry of somatic hypermutation. *Annu. Rev. Immunol.* 26:481–511. https://doi.org/10.1146/annurev.immunol.26.021607.090236

Petersen-Mahrt, S.K., R.S. Harris, and M.S. Neuberger. 2002. AID mutates E. coli suggesting a DNA deamination mechanism for antibody diversification. *Nature.* 418:99–103. https://doi.org/10.1038/nature00862

Pham, P., R. Bransteitter, J. Petruska, and M.F. Goodman. 2003. Processive AID-catalysed cytosine deamination on single-stranded DNA simulates somatic hypermutation. *Nature.* 424:103–107. https://doi.org/10.1038/nature01760

Powell, J.D., K.N. Pollizzi, E.B. Heikamp, and M.R. Horton. 2012. Regulation of immune responses by mTOR. *Annu. Rev. Immunol.* 30:39–68. https://doi.org/10.1146/annurev-immunol-020711-075024

Puthalakath, H., L.A. O'Reilly, P. Gunn, L. Lee, P.N. Kelly, N.D. Huntington, P.D. Hughes, E.M. Michalak, J. McKimm-Breschkin, N. Motoyama, et al. 2007. ER stress triggers apoptosis by activating BH3-only protein Bim. *Cell.* 129:1337–1349. https://doi.org/10.1016/j.cell.2007.04.027

Quirós, P.M., M.A. Prado, N. Zamboni, D. D'Amico, R.W. Williams, D. Finley, S.P. Gygi, and J. Auwerx. 2017. Multi-omics analysis identifies ATF4 as a key regulator of the mitochondrial stress response in mammals. *J. Cell Biol.* 216:2027–2045. https://doi.org/10.1083/jcb.201702058

Ramiro, A.R., P. Stavropoulos, M. Jankovic, and M.C. Nussenzweig. 2003. Transcription enhances AID-mediated cytidine deamination by exposing single-stranded DNA on the nontemplate strand. *Nat. Immunol.* 4: 452–456. https://doi.org/10.1038/ni920

Reboldi, A., and J.G. Cyster. 2016. Peyer's patches: organizing B-cell responses at the intestinal frontier. *Immunol. Rev.* 271:230–245. https://doi.org/10.1111/imr.12400

Rendleman, J., Z. Cheng, S. Maity, N. Kastelic, M. Munschauer, K. Allgoewer, G. Teo, Y.B.M. Zhang, A. Lei, B. Parker, et al. 2018. New insights into the cellular temporal response to proteostatic stress. *eLife.* 7. e39054. https://doi.org/10.7554/eLife.39054

Revy, P., T. Muto, Y. Levy, F. Geissmann, A. Plebani, O. Sanal, N. Catalan, M. Forveille, R. Dufourcq-Labelouse, A. Gennery, et al. 2000. Activation-induced cytidine deaminase (AID) deficiency causes the autosomal recessive form of the Hyper-IgM syndrome (HIGM2). *Cell.* 102:565–575. https://doi.org/10.1016/S0092-8674(00)00079-9

Rickert, R.C., J. Roes, and K. Rajewsky. 1997. B lymphocyte-specific, Cre-mediated mutagenesis in mice. *Nucleic Acids Res.* 25:1317–1318. https://doi.org/10.1093/nar/25.6.1317

Robinson, M.D., D.J. McCarthy, and G.K. Smyth. 2010. edgeR: a Bioconductor package for differential expression analysis of digital gene expression data. *Bioinformatics.* 26:139–140. https://doi.org/10.1093/bioinformatics/btp616

Roco, J.A., L. Mesin, S.C. Binder, C. Nefzger, P. Gonzalez-Figueroa, P.F. Canete, J. Ellyard, Q. Shen, P.A. Robert, J. Cappello, et al. 2019. Class-Switch Recombination Occurs Infrequently in Germinal Centers. *Immunity.* 51:337–350.e7. https://doi.org/10.1016/j.immuni.2019.07.001

Ron, D., and P. Walter. 2007. Signal integration in the endoplasmic reticulum unfolded protein response. *Nat. Rev. Mol. Cell Biol.* 8:519–529. https://doi.org/10.1038/nrm2199

Roth, D.B.. 2014. V(D)J Recombination: Mechanism, Errors, and Fidelity. *Microbiol. Spectr.* 2:1–11. https://doi.org/10.1128/microbiolspec.MDNA3-0041-2014

Rouaud, P., C. Vincent-Fabert, A. Saintamand, R. Fiancette, M. Marquet, I. Robert, B. Reina-San-Martin, E. Pinaud, M. Cogné, and Y. Denizot. 2013. The IgH 3′ regulatory region controls somatic hypermutation in germinal center B cells. *J. Exp. Med.* 210:1501–1507. https://doi.org/10.1084/jem.20130072

Rzymski, T., M. Milani, L. Pike, F. Buffa, H.R. Mellor, L. Winchester, I. Pires, E. Hammond, I. Ragoussis, and A.L. Harris. 2010. Regulation of autophagy by ATF4 in response to severe hypoxia. *Oncogene.* 29: 4424–4435. https://doi.org/10.1038/onc.2010.191

Sala, C., G. Mattiuz, S. Pietrobono, A. Chicca, and S.G. Conticello. 2015. Splice variants of activation induced deaminase (AID) do not affect the efficiency of class switch recombination in murine CH12F3 cells. *PLoS One.* 10. e0121719. https://doi.org/10.1371/journal.pone.0121719

Sander, S., V.T. Chu, T. Yasuda, A. Franklin, R. Graf, D.P. Calado, S. Li, K. Imami, M. Selbach, M. Di Virgilio, et al. 2015. PI3 Kinase and FOXO1 Transcription Factor Activity Differentially Control B Cells in the Germinal Center Light and Dark Zones. *Immunity.* 43:1075–1086. https://doi.org/10.1016/j.immuni.2015.10.021

Sayegh, C.E., M.W. Quong, Y. Agata, and C. Murre. 2003. E-proteins directly regulate expression of activation-induced deaminase in mature B cells. *Nat. Immunol.* 4:586–593. https://doi.org/10.1038/ni923

Scheuner, D., B. Song, E. McEwen, C. Liu, R. Laybutt, P. Gillespie, T. Saunders, S. Bonner-Weir, and R.J. Kaufman. 2001. Translational control is required for the unfolded protein response and in vivo glucose homeostasis. *Mol. Cell.* 7:1165–1176. https://doi.org/10.1016/S1097-2765(01)00265-9

Schröder, M., and R.J. Kaufman. 2005. The mammalian unfolded protein response. *Annu. Rev. Biochem.* 74:739–789. https://doi.org/10.1146/annurev.biochem.73.011303.074134

Sernández, I.V., V.G. de Yébenes, Y. Dorsett, and A.R. Ramiro. 2008. Haploinsufficiency of activation-induced deaminase for antibody diversification and chromosome translocations both in vitro and in vivo. *PLoS One.* 3. e3927. https://doi.org/10.1371/journal.pone.0003927

Shaffer, A.L., M. Shapiro-Shelef, N.N. Iwakoshi, A.H. Lee, S.B. Qian, H. Zhao, X. Yu, L. Yang, B.K. Tan, A. Rosenwald, et al. 2004. XBP1, downstream of Blimp-1, expands the secretory apparatus and other organelles, and increases protein synthesis in plasma cell differentiation. *Immunity.* 21: 81–93. https://doi.org/10.1016/j.immuni.2004.06.010

Sharma, V.K., A. Singh, S.K. Srivastava, V. Kumar, N.L. Gardi, A. Nalwa, A.K. Dinda, P. Chattopadhyay, and S. Yadav. 2016. Increased expression of platelet-derived growth factor associated protein-1 is associated with PDGF-B mediated glioma progression. *Int. J. Biochem. Cell Biol.* 78: 194–205. https://doi.org/10.1016/j.biocel.2016.07.016

Shen, L., K.P. Huang, H.C. Chen, and F.L. Huang. 1996. Molecular cloning and characterization of a novel casein kinase II substrate, HASPP28, from rat brain. *Arch. Biochem. Biophys.* 327:131–141. https://doi.org/10.1006/abbi.1996.0101

Shi, W., Y. Liao, S.N. Willis, N. Taubenheim, M. Inouye, D.M. Tarlinton, G.K. Smyth, P.D. Hodgkin, S.L. Nutt, and L.M. Corcoran. 2015. Transcriptional profiling of mouse B cell terminal differentiation defines a signature for antibody-secreting plasma cells. *Nat. Immunol.* 16:663–673. https://doi.org/10.1038/ni.3154

Sohail, A., J. Klapacz, M. Samaranayake, A. Ullah, and A.S. Bhagwat. 2003. Human activation-induced cytidine deaminase causes transcription-dependent, strand-biased C to U deaminations. *Nucleic Acids Res.* 31: 2990–2994. https://doi.org/10.1093/nar/gkg464

Stockdale, A.M., J.L. Dul, D.L. Wiest, M. Digel, and Y. Argon. 1987. The expression of membrane and secreted immunoglobulin during the in vitro differentiation of the murine B cell lymphoma CH12. *J. Immunol.* 139: 3527–3535.

Takizawa, M., H. Tolarová, Z. Li, W. Dubois, S. Lim, E. Callen, S. Franco, M. Mosaico, L. Feigenbaum, F.W. Alt, et al. 2008. AID expression levels determine the extent of cMyc oncogenic translocations and the incidence of B cell tumor development. *J. Exp. Med.* 205:1949–1957. https://doi.org/10.1084/jem.20081007

Taubenheim, N., D.M. Tarlinton, S. Crawford, L.M. Corcoran, P.D. Hodgkin, and S.L. Nutt. 2012. High rate of antibody secretion is not integral to plasma cell differentiation as revealed by XBP-1 deficiency. *J. Immunol.* 189:3328–3338. https://doi.org/10.4049/jimmunol.1201042

Tellier, J., W. Shi, M. Minnich, Y. Liao, S. Crawford, G.K. Smyth, A. Kallies, M. Busslinger, and S.L. Nutt. 2016. Blimp-1 controls plasma cell function through the regulation of immunoglobulin secretion and the unfolded protein response. *Nat. Immunol.* 17:323–330. https://doi.org/10.1038/ni.3348

Teng, G., P. Hakimpour, P. Landgraf, A. Rice, T. Tuschl, R. Casellas, and F.N. Papavasiliou. 2008. MicroRNA-155 is a negative regulator of activation-

induced cytidine deaminase. *Immunity*. 28:621–629. https://doi.org/10.1016/j.immuni.2008.03.015

Teske, B.F., M.E. Fusakio, D. Zhou, J. Shan, J.N. McClintick, M.S. Kilberg, and R.C. Wek. 2013. CHOP induces activating transcription factor 5 (ATF5) to trigger apoptosis in response to perturbations in protein homeostasis. *Mol. Biol. Cell*. 24:2477–2490. https://doi.org/10.1091/mbc.e13-01-0067

Tirasophon, W., A.A. Welihinda, and R.J. Kaufman. 1998. A stress response pathway from the endoplasmic reticulum to the nucleus requires a novel bifunctional protein kinase/endoribonuclease (Ire1p) in mammalian cells. *Genes Dev*. 12:1812–1824. https://doi.org/10.1101/gad.12.12.1812

Todd, D.J., L.J. McHeyzer-Williams, C. Kowal, A.H. Lee, B.T. Volpe, B. Diamond, M.G. McHeyzer-Williams, and L.H. Glimcher. 2009. XBP1 governs late events in plasma cell differentiation and is not required for antigen-specific memory B cell development. *J. Exp. Med*. 206:2151–2159. https://doi.org/10.1084/jem.20090738

Trendel, J., T. Schwarzl, R. Horos, A. Prakash, A. Bateman, M.W. Hentze, and J. Krijgsveld. 2019. The Human RNA-Binding Proteome and Its Dynamics during Translational Arrest. *Cell*. 176:391–403.e19. https://doi.org/10.1016/j.cell.2018.11.004

van Anken, E., E.P. Romijn, C. Maggioni, A. Mezghrani, R. Sitia, I. Braakman, and A.J.R. Heck. 2003. Sequential waves of functionally related proteins are expressed when B cells prepare for antibody secretion. *Immunity*. 18:243–253. https://doi.org/10.1016/S1074-7613(03)00024-4

van Maldegem, F., R.A. Jibodh, R. van Dijk, R.J. Bende, and C.J.M. van Noesel. 2010. Activation-induced cytidine deaminase splice variants are defective because of the lack of structural support for the catalytic site. *J. Immunol*. 184:2487–2491. https://doi.org/10.4049/jimmunol.0903102

van Maldegem, F., F.A. Scheeren, R. Aarti Jibodh, R.J. Bende, H. Jacobs, and C.J. van Noesel. 2009. AID splice variants lack deaminase activity. *Blood*. 113:1862–1864, author reply :1864. https://doi.org/10.1182/blood-2008-08-175265

Victora, G.D., and M.C. Nussenzweig. 2012. Germinal centers. *Annu. Rev. Immunol*. 30:429–457. https://doi.org/10.1146/annurev-immunol-020711-075032

Walter, P., and D. Ron. 2011. The unfolded protein response: from stress pathway to homeostatic regulation. *Science*. 334:1081–1086. https://doi.org/10.1126/science.1209038

Wang, Q., H. Mora-Jensen, M.A. Weniger, P. Perez-Galan, C. Wolford, T. Hai, D. Ron, W. Chen, W. Trenkle, A. Wiestner, et al. 2009. ERAD inhibitors integrate ER stress with an epigenetic mechanism to activate BH3-only protein NOXA in cancer cells. *Proc. Natl. Acad. Sci. USA*. 106:2200–2205. https://doi.org/10.1073/pnas.0807611106

Wang, X.Z., H.P. Harding, Y. Zhang, E.M. Jolicoeur, M. Kuroda, and D. Ron. 1998. Cloning of mammalian Ire1 reveals diversity in the ER stress responses. *EMBO J*. 17:5708–5717. https://doi.org/10.1093/emboj/17.19.5708

Weston, V.J., W. Wei, T. Stankovic, and P. Kearns. 2018. Synergistic action of dual IGF1/R and MEK inhibition sensitizes childhood acute lymphoblastic leukemia (ALL) cells to cytotoxic agents and involves down-regulation of STAT6 and PDAP1. *Exp. Hematol*. 63:52–63.e5. https://doi.org/10.1016/j.exphem.2018.04.002

Wiest, D.L., J.K. Burkhardt, S. Hester, M. Hortsch, D.I. Meyer, and Y. Argon. 1990. Membrane biogenesis during B cell differentiation: most endoplasmic reticulum proteins are expressed coordinately. *J. Cell Biol*. 110:1501–1511. https://doi.org/10.1083/jcb.110.5.1501

Wurmus, R., B. Uyar, B. Osberg, V. Franke, A. Gosdschan, K. Wreczycka, J. Ronen, and A. Akalin. 2018. PiGx: reproducible genomics analysis pipelines with GNU Guix. *Gigascience*. 7:1–14. https://doi.org/10.1093/gigascience/giy123

Xu, G., J.R. Chapman, I. Brandsma, J. Yuan, M. Mistrik, P. Bouwman, J. Bartkova, E. Gogola, D. Warmerdam, M. Barazas, et al. 2015. REV7 counteracts DNA double-strand break resection and affects PARP inhibition. *Nature*. 521:541–544. https://doi.org/10.1038/nature14328

Ye, J., M. Kumanova, L.S. Hart, K. Sloane, H. Zhang, D.N. De Panis, E. Bobrovnikova-Marjon, J.A. Diehl, D. Ron, and C. Koumenis. 2010. The GCN2-ATF4 pathway is critical for tumour cell survival and proliferation in response to nutrient deprivation. *EMBO J*. 29:2082–2096. https://doi.org/10.1038/emboj.2010.81

Yoshida, H., T. Matsui, A. Yamamoto, T. Okada, and K. Mori. 2001. XBP1 mRNA is induced by ATF6 and spliced by IRE1 in response to ER stress to produce a highly active transcription factor. *Cell*. 107:881–891. https://doi.org/10.1016/S0092-8674(01)00611-0

Zhang, K., H.N. Wong, B. Song, C.N. Miller, D. Scheuner, and R.J. Kaufman. 2005. The unfolded protein response sensor IRE1alpha is required at 2 distinct steps in B cell lymphopoiesis. *J. Clin. Invest*. 115:268–281. https://doi.org/10.1172/JCI200521848

Zhou, C., A. Saxon, and K. Zhang. 2003. Human activation-induced cytidine deaminase is induced by IL-4 and negatively regulated by CD45: implication of CD45 as a Janus kinase phosphatase in antibody diversification. *J. Immunol*. 170:1887–1893. https://doi.org/10.4049/jimmunol.170.4.1887

Zhu, H., B. Bhatt, S. Sivaprakasam, Y. Cai, S. Liu, S.K. Kodeboyina, N. Patel, N.M. Savage, A. Sharma, R.J. Kaufman, et al. 2019. Ufbp1 promotes plasma cell development and ER expansion by modulating distinct branches of UPR. *Nat. Commun*. 10:1084. https://doi.org/10.1038/s41467-019-08908-5

Zou, W., P. Yue, F.R. Khuri, and S.Y. Sun. 2008. Coupling of endoplasmic reticulum stress to CDDO-Me-induced up-regulation of death receptor 5 via a CHOP-dependent mechanism involving JNK activation. *Cancer Res*. 68:7484–7492. https://doi.org/10.1158/0008-5472.CAN-08-1318

JEM

Supplemental material

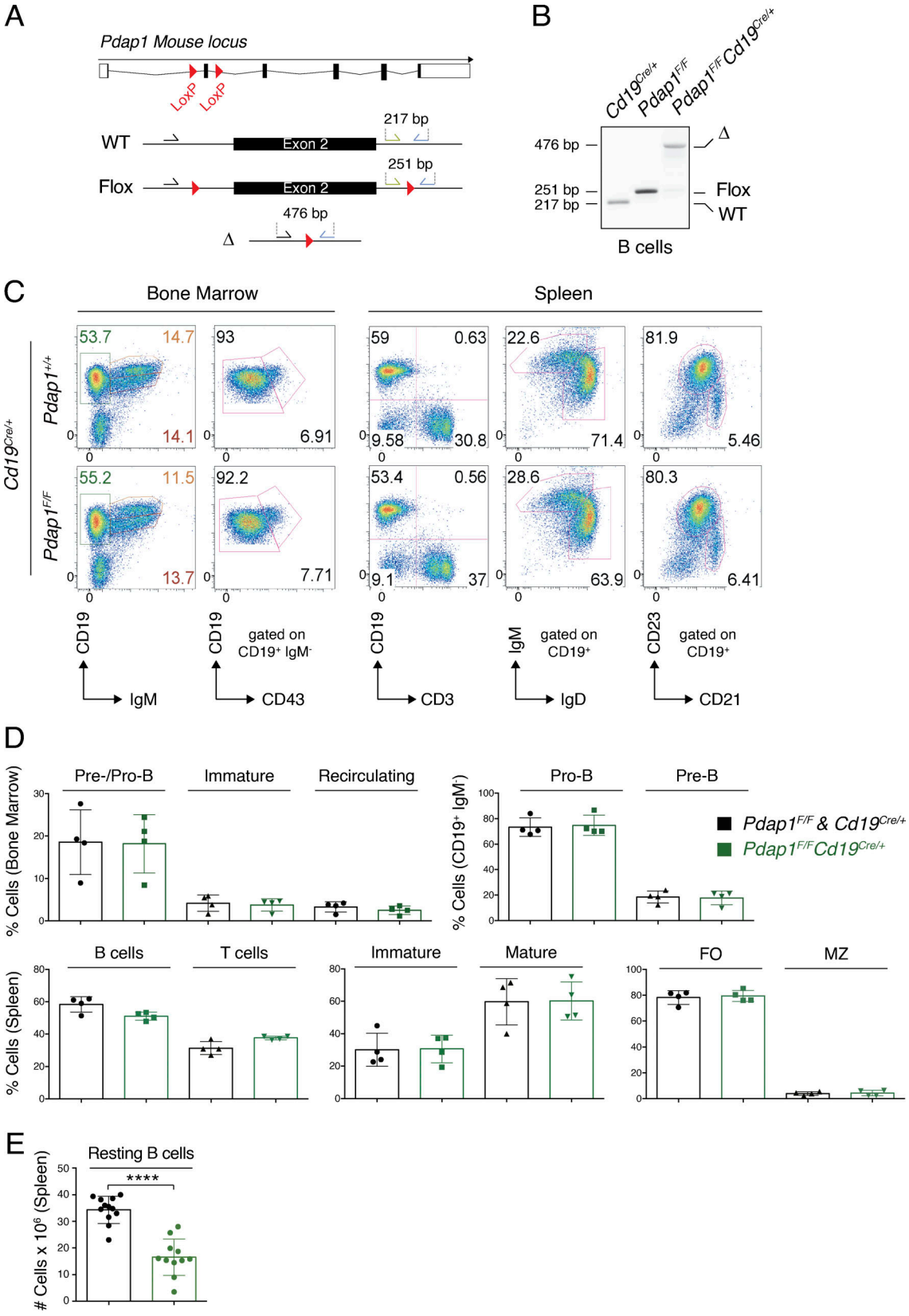

Figure S1. **Pdap1 is largely dispensable for B cell development. (A)** Schematic representation of *Pdap1* locus and genotyping strategy. WT, WT *Pdap1* allele; Flox, conditional *Pdap1* allele; Δ, null *Pdap1* allele. **(B)** Electrophoretic analysis of *Pdap1* allele status in resting splenic B cells isolated from mice of the indicated genotype. **(C)** Representative flow cytometry analysis of lymphoid tissues from control and $Pdap1^{F/F}Cd19^{Cre/+}$ mice. **(D)** Summary graphs for four mice per genotype. **(E)** Number of resting B cells isolated from spleens of the indicated genotype. Each dot represents a different mouse. Significance in D and E was calculated with the Mann–Whitney *U* test, and error bars represent SD. No difference among groups was significant for graphs in D. ****, P ≤ 0.0001.

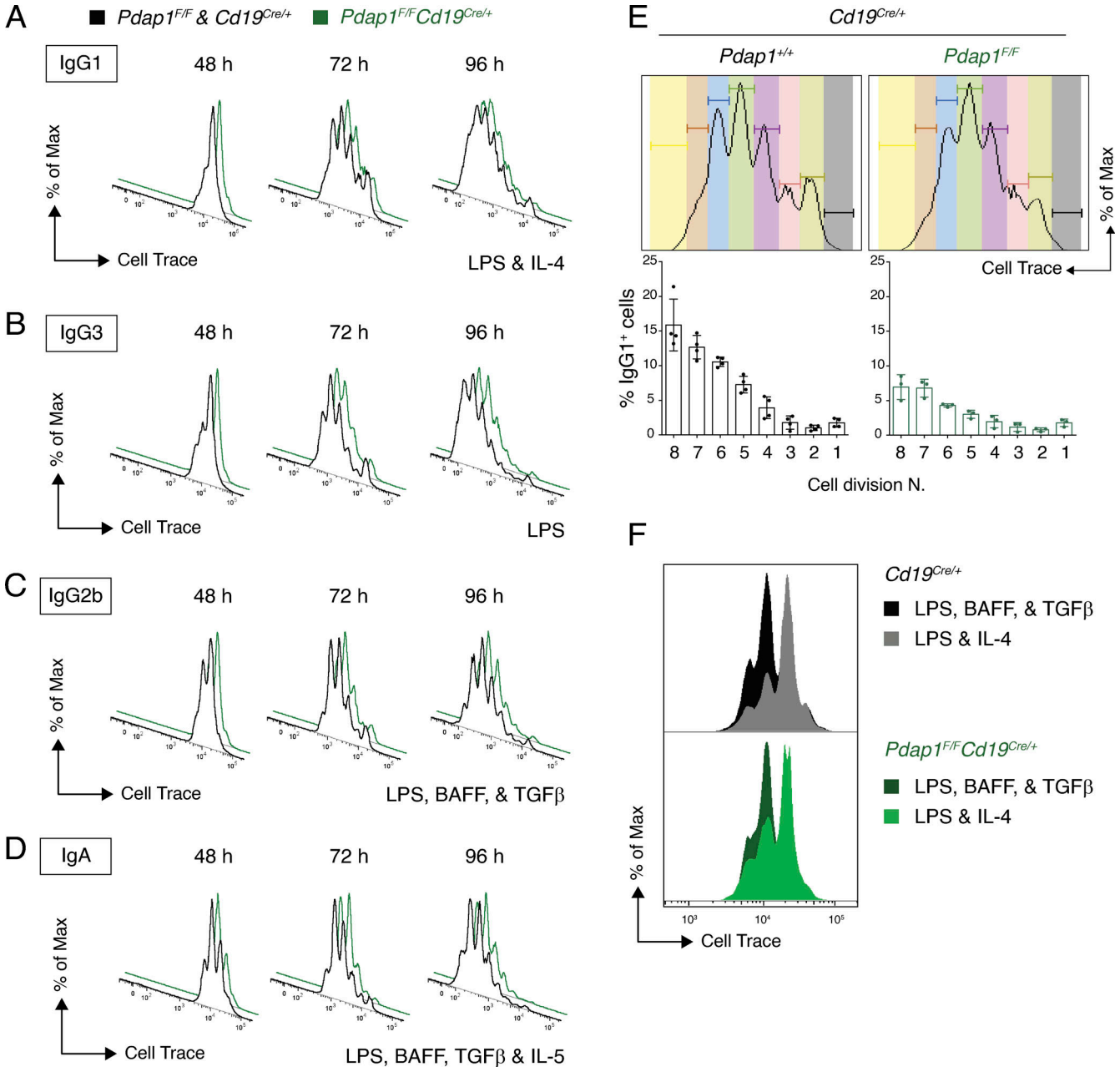

Figure S2. **Pdap1 is dispensable for B cell proliferation. (A–D)** Proliferation analysis by CellTrace Violet dilution of primary cultures of *Cd19*$^{Cre/+}$ and *Pdap1*$^{F/F}$*Cd19*$^{Cre/+}$ B lymphocytes stimulated with LPS-IL-4 (A), LPS only (B), LPS-BAFF-TGFβ (C), or LPS-BAFF-TGFβ-IL-5 (D). Data are representative of at least two mice per genotype. **(E)** Graph showing percentage of IgG1$^+$ cells per cell division in primary cultures of *Cd19*$^{Cre/+}$ and *Pdap1*$^{F/F}$*Cd19*$^{Cre/+}$ splenocytes stimulated with LPS and IL-4 for 72 h. Graph summarizes at least three mice per genotype, and error bars represent SD. Representative cell division plots as measured by CellTrace Violet dilution are shown on top. **(F)** Representative overlay of CellTrace Violet proliferation tracks of LPS-IL-4 and LPS-BAFF-TGFβ cultures 48 h after activation.

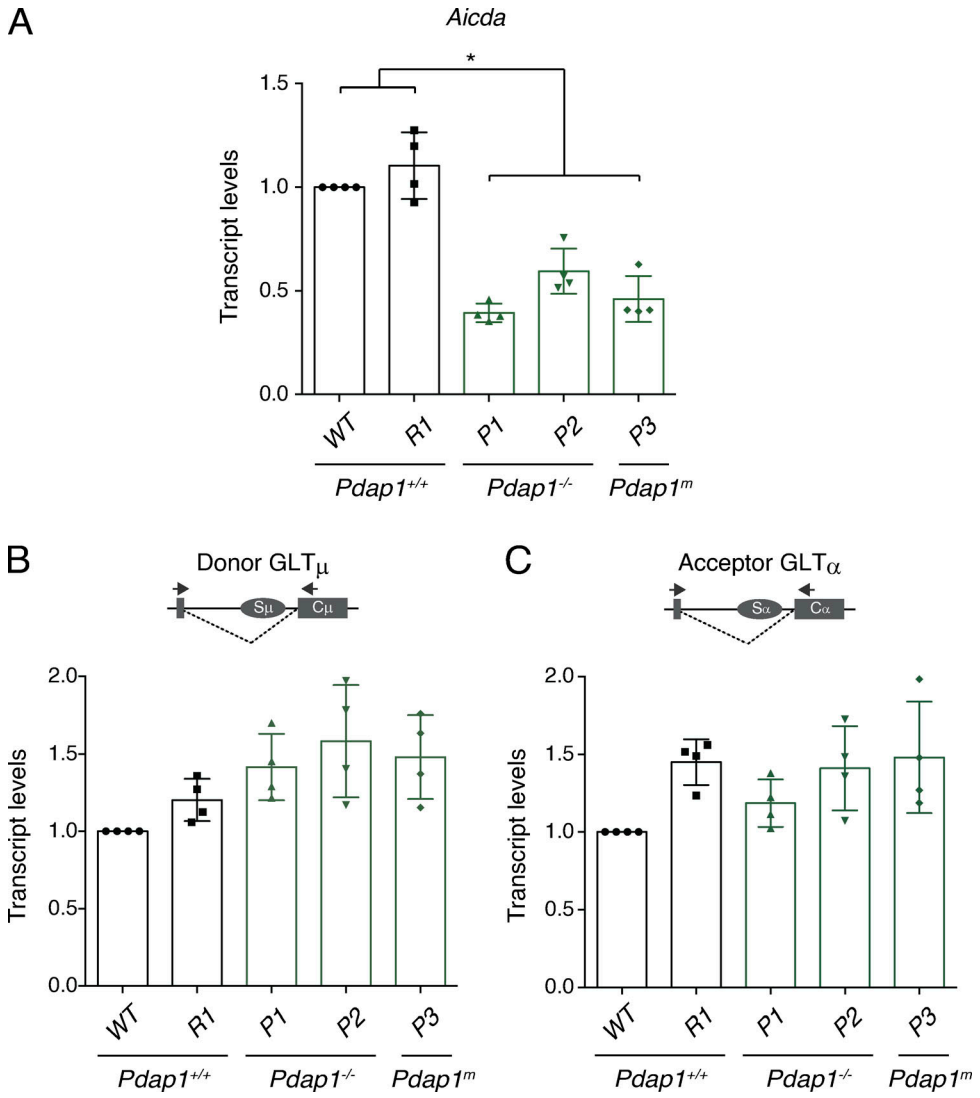

Figure S3. ***Aicda* mRNA levels are reduced in Pdap1-deficient CH12 cell lines. (A)** qPCR analysis for *Aicda* mRNA in activated CH12 cell lines of the indicated genotypes. Graph summarizes four independent experiments. Parental WT CH12 cells within each experiment were assigned an arbitrary value of 1. **(B and C)** qPCR analysis for Igμ (B) and Igα (C) GLT levels in activated CH12 cell lines of the indicated genotypes. The schematic representations on top of each graph indicate the location of primers used to analyze postspliced germline transcripts. Graphs summarize four independent experiments. Parental WT CH12 cells within each experiment were assigned an arbitrary value of 1. Significance in A was calculated with the Mann–Whitney *U* test. Error bars represent SD. *, $P \leq 0.05$.

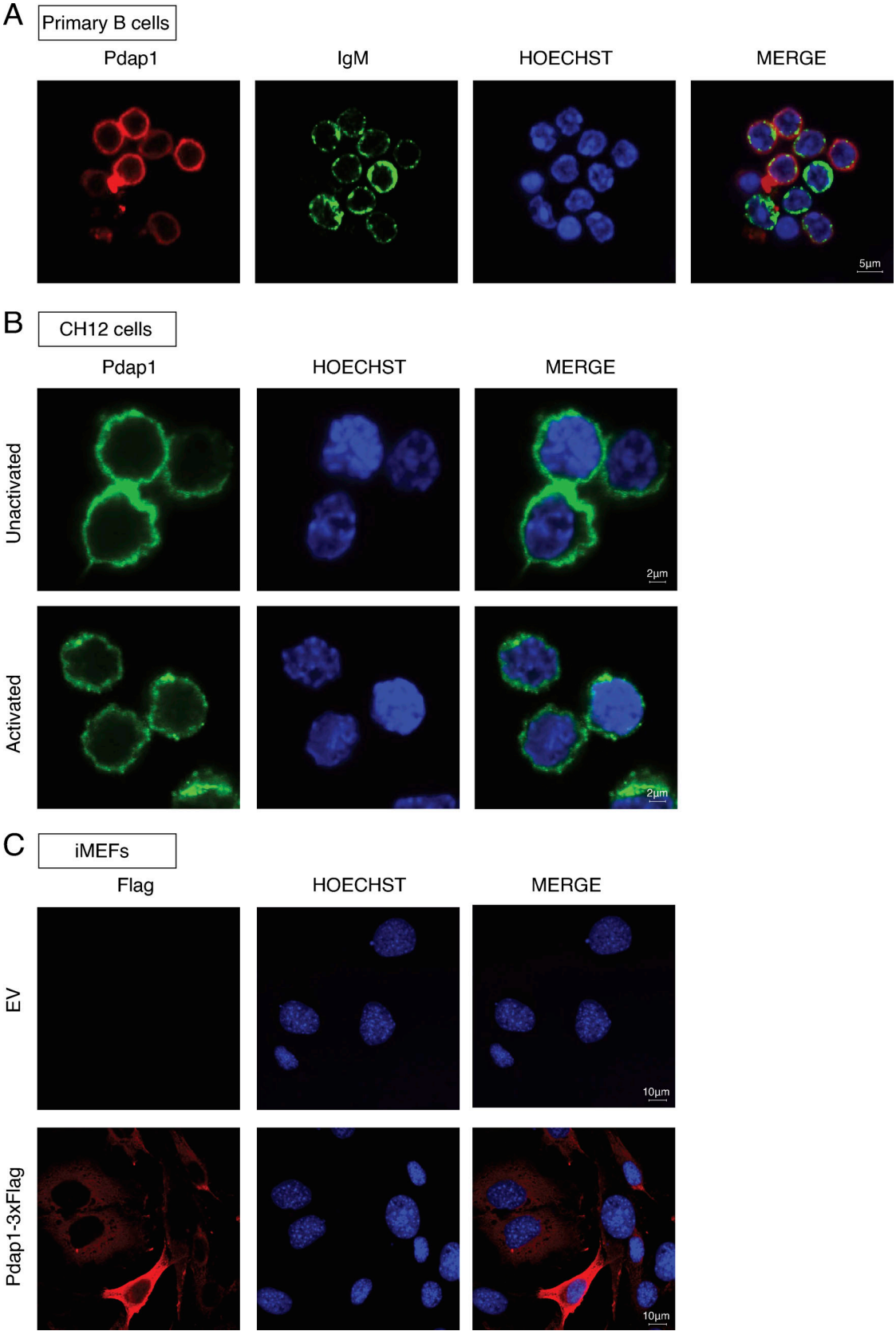

Figure S4. **Pdap1 is localized primarily in the cytoplasm. (A–C)** Immunofluorescence staining of Pdap1 in WT primary B cells (resting splenocytes; A), CH12 (unactivated and 48 h after activation; B), and iMEFs (C). Staining is against endogenous Pdap1 in A and B and Pdap1-3xFlag in C. EV, empty vector. Scale bars in A–C indicate 5, 2, and 10 μm, respectively.

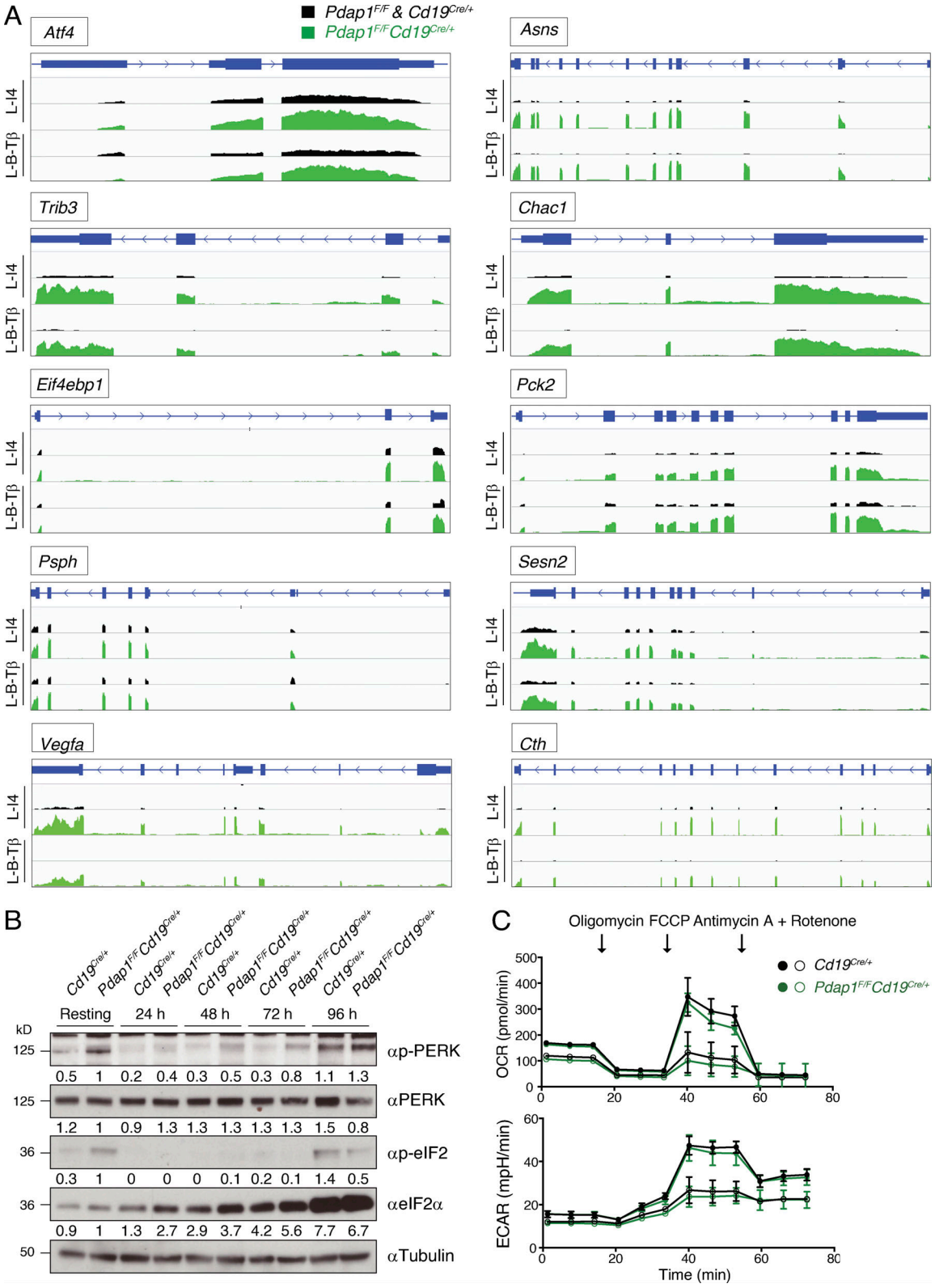

Figure S5. **Stress response signature of Pdap1-deficient B cells. (A)** Coverage of stress response genes in B cells of the indicated genotypes 48 h after activation with LPS and IL-4 (L-I4) or LPS, BAFF, and TGFβ (L-B-Tβ), as measured by RNA-seq analysis. 10 selected genes are shown. **(B)** WB analysis as in Fig. 5 D for an independent mouse pair (control and *Pdap1*$^{F/F}$*Cd19*$^{Cre/+}$). Splenocytes were isolated (resting B cells) and activated for 24–96 h with LPS and IL-4. Quantification values of WB signals are indicated underneath the corresponding blots. **(C)** Graphs showing oxygen consumption rate (OCR) and extracellular acidification rate (ECAR) analysis of resting primary B cell cultures. Filled and empty symbols indicate 10^6 or 0.5×10^6 cells/well seeding densities, respectively. Each data point represents the mean of three independent measurements, with error bars indicating SD. Labeled arrows denote injections of the indicated agents.

Table S1 shows a pairwise comparison of differentially regulated genes in control versus *Pdap1*$^{F/F}$*Cd19*$^{CRE/+}$ splenocytes. Table S2 lists the oligonucleotides used in this study.